Remote Sensing of Environment 295 (2023) 113665

Contents lists available at ScienceDirect

Remote Sensing of Environment

journal homepage: www.elsevier.com/locate/rse

Evaluating the saturation effect of vegetation indices in forests using 3D radiative transfer simulations and satellite observations

Si Gao [a,b], Run Zhong [b], Kai Yan [a,b,*], Xuanlong Ma [c,**], Xinkun Chen [b], Jiabin Pu [d], Sicong Gao [e], Jianbo Qi [a], Gaofei Yin [f], Ranga B. Myneni [d]

[a] Center for GeoData and Analysis, State Key Laboratory of Remote Sensing Science, Faculty of Geographical Science, Beijing Normal University, Beijing 100875, China
[b] School of Land Science and Techniques, China University of Geosciences, Beijing 100083, China
[c] College of Earth and Environmental Sciences, Lanzhou University, Lanzhou 730020, China
[d] Department of Earth and Environment, Boston University, Boston, MA 02215, USA
[e] Land and Water, Commonwealth Scientific and Industrial Research Organization, Adelaide, SA 5064, Australia
[f] Faculty of Geosciences and Environmental Engineering, Southwest Jiaotong University, Chengdu 610031, China

ARTICLE INFO

Edited by Jing M. Chen

Keywords:
Vegetation indices (VI)
Leaf area index (LAI)
Saturation effect
Vegetation canopy
Three-dimensional radiative transfer (3D RT) model

ABSTRACT

Vegetation indices (VIs) have been used extensively for qualitative and quantitative remote sensing monitoring of vegetation vigor and growth dynamics. However, the saturation phenomenon of VIs (i.e., insignificant change at moderate to high vegetation densities) poses a known limitation to their ability to characterize surface vegetation over the dense canopy. Although the mechanisms underlying saturation are relatively straightforward and several VIs have been proposed to mitigate the saturation effect, the assessment of the saturation effect of VIs remains insufficient. Notably, no unified metric has been proposed to quantify the VI saturation phenomenon, limiting VI selection in practical applications. In this study, we proposed two indicators to describe the saturation phenomenon and utilized a well-validated three-dimensional (3D) canopy radiative transfer (RT) model large-scale remote sensing data and image simulation framework (LESS) to simulate the bidirectional reflectance factor (BRF) of six forests scenes and assessed the variations in VIs in relation to leaf area index (LAI) values over different backgrounds, sun-sensor geometries, and spatial distribution types. The saturation characteristics of 36 VIs were evaluated in combination with simulation results and satellite observations from multiple sensors. The ranking of VI saturation from simulated and satellite results revealed a good agreement. Our results indicated that the simple ratio vegetation index (SR) performed best with the highest saturation point and can well characterize the surface vegetation condition until LAI reaches 4. Besides, we found that the saturation effect of VIs was influenced by soil brightness, sun-sensor geometry, and canopy structure. SR, modified simple ratio (MSR) and normalized green red difference index (NGRDI) were the most susceptible to these disturbing factors, although they had higher resistance to saturation. Modified triangular vegetation index 1 (MTVI1), modified non-linear vegetation index (MNLI), triangular greenness index (TGI), and triangular vegetation index (TriVI) performed well overall, combining the ability to resist saturation and disturbance factors. Appropriate application of VIs can help better understand vegetation responses to climate change and accurately assess ecosystem status. Our results contribute to the understanding of the VI saturation effect and provide a combined model and satellite data experimental workflow in appropriate VI selection to accurately characterize vegetation.

1. Introduction

Remote sensing has emerged as an essential tool for monitoring vegetation dynamics because of its ability to take repeatable measurements over large spatial and long temporal scales (Huang et al., 2020; Jiang et al., 2006). As a simple mathematical transformation of spectral bands, vegetation indices (VIs) are designed to enhance the contribution of vegetation properties, which can be computed directly without any bias or assumptions regarding land cover classes, soil types, or climatic conditions (Huete et al., 2002). Numerous studies have offered

* Corresponding author at: Faculty of Geographical Science, Beijing Normal University, Beijing 100875, China.
** Corresponding author.
E-mail addresses: kaiyan@bnu.edu.cn (K. Yan), xlma@lzu.edu.cn (X. Ma).

https://doi.org/10.1016/j.rse.2023.113665
Received 1 April 2023; Received in revised form 26 May 2023; Accepted 4 June 2023
Available online 14 June 2023

considerable evidence that VIs strongly correlate with vegetation structural, phenological, and biophysical parameters, such as leaf area index (LAI) (Cao et al., 2017; Potithep et al., 2013; Xing et al., 2020), fractional vegetation cover (Gao et al., 2020; Yan et al., 2020), fraction of absorbed photosynthetically active radiation (Kerr and Ostrovsky, 2003), and gross primary production (GPP) (Ma et al., 2014).

While being widely used, some concerns about VIs remain to be resolved, and one of them is saturation, or lack of sensitivity, to moderate-dense canopy conditions (Huete et al., 2002; Weiss and Baret, 1999; Zhao et al., 2012). The saturation effect is an inevitable phenomenon for all VIs and leads to underestimating ecosystem productivity in densely vegetated areas (i.e., high LAI areas) (Aklilu Tesfaye and Gessesse Awoke, 2021; Huete et al., 1997; Mutanga and Skidmore, 2004). Taking the normalized difference vegetation index (NDVI) as an example, NDVI asymptotically reaches saturation when LAI exceeds 2 $m^2 m^{-2}$, and yields poor estimates of vegetation parameters. Even if the ground vegetation continues to grow, NDVI does not increase with or only slight changes and therefore has limited value in assessing biomass during the peak of seasons (Haboudane et al., 2004).

The saturation effect of VIs varies greatly among biomes and is more likely to occur in forests with complex spatial heterogeneity (Baloloy et al., 2018). Gao et al. pointed out that NDVI approaches a saturation level in forests when LAI is higher than 3 $m^2 m^{-2}$ (Gao et al., 2000). However, Typically LAI is in the range of 5–7 in temperate broad-leaved forests and 6–8 in lowland tropical forests (Leigh, 1999). It's readily apparent that the saturation effect directly limits the application and phenological detection of VIs, and using remotely sensed NDVI as an accurate proxy of forest development is controversial (Köhler et al., 2018; Zhang et al., 2016). Therefore, more attention needs to be paid to the saturation effects of VIs in forests.

Several approaches have been developed to mitigate the saturation effect of VIs, which can be split into two groups. One group of methods focused on changing the mathematical forms or improving existing VI by incorporating additional variables. For example, the wide dynamic range vegetation index (WDRVI) (Gitelson, 2004) and modified NDVI (MNDVI) (Vaiopoulos et al., 2004) were generated by adding weighting factors to near-infrared (NIR) reflectance into the NDVI equation to adjust the relative contribution between NIR and red band contributions, and therefore improve saturation resistance; plant phenology index (PPI) (Jin and Eklundh, 2014) was developed based on modified Beer's law, which largely enhances the linear relationship with surface LAI due to its physical-based advantages. However, these methods typically require additional coefficients, and selecting a suitable value is also a matter of consideration. The other category of methods is particularly focused on creating novel VIs by considering more spectral information, such as photochemical reflectance index (PRI) (Gamon et al., 1992), chlorophyll/carotenoid index (CCI) (Gamon et al., 2016) and red-edge NDVI (NDVIre) (Gitelson and Merzlyak, 1994). These methods could achieve greater sensitivity in high biomass situations, but also place higher demands for sensors. Moreover, non-linear relationships between all VIs and vegetation biophysical parameters are unavoidable owing to the fact that saturation is an inherent property of reflectance. Therefore, a full saturation assessment of the existing, simple wide-band VIs is highly desirable.

Numerous studies have assessed the VIs saturation phenomenon and offered important conclusions, but the assessments are still inadequate, especially the lack of a clear indicator of the saturation phenomenon. For almost all VIs, the sensitivity to LAI becomes weaker as the LAI increases, and beyond a threshold, it stops growing, so it can be classified as sensitive, insensitive, or unresponsive depending on the level of vegetation density (Carlson and Ripley, 1997; Jiang and Huete, 2010). It is crucial to describe this progressive process of VI saturation with quantitative metrics, which can guide the selecting VI for specific applications or proposing new VIs.

The approaches for analyzing the VI saturation effect can be classified into two types: observation-based and model-based. A wealth of observations from multiple platforms (e.g., satellites, drones, ground) are available to assess saturation phenomena in real scenes, and several important conclusions have been drawn (Aklilu Tesfaye and Gessesse Awoke, 2021; Huete et al., 1997). However, their accuracy is easily affected by confounding factors, such as atmospheric conditions and measurement errors. Given the complexities of mixed landscapes and the interplay of these confounding factors, it is difficult to disentangle these effects by merely using observations (Glenn et al., 2008; Pu et al., 2020), and hence cannot make a definitive assessment of the impact of different factors on saturation effect.

Simulation-based approaches could well complement observation methods with the support of radiative transfer models (RTM) that establish an explicit connection between LAI and VI based on the physical laws of photon transport within the vegetation canopy (Fang and Liang, 2003). RTM can accurately simulate the radiation properties of realistic landscapes under various conditions, however, vegetation types must be fully accounted for when choosing a RTM (Myneni et al., 2002; Yao et al., 2008). One-dimensional (1D) RTMs (e.g., SAIL (Verhoef, 1984) and SCOPE (Van Der Tol et al., 2009)) assume that canopy is horizontally homogeneous and semi-infinite layers and fail to accurately describe the canopy structure and spatial distribution and spatial structure. Therefore, they are more broadly applicable to continuous canopies like grasslands and croplands. Besides, previous studies have demonstrated that 1D RT can exhibit significant biases in-comparison to more accurate three-dimensional (3D) RTMs and observations, yielding a potential significant underestimation of global photosynthesis in Earth system models (Braghiere et al., 2019; Kobayashi et al., 2012). 3D RTMs (e.g., DART (Etchegorry et al., 2015), Rayspread (Widlowski et al., 2006), and FLiES (Kobayashi and Iwabuchi, 2008)) offer a more refined depiction of the tree structure and can well simulate multiple scattering, so they are suitable for the assessment of forest scenes with complex spatial heterogeneity (Regaieg et al., 2021; Wang et al., 2015). While 3D RT simulations are highly accurate and can be a promising alternative for saturation effect analysis, their application potential has not been fully realized due to their computational complexity. In recent years, continuous advances in both computing efficiency and 3D RTMs have provided an excellent opportunity to re-examine the saturation effect of VIs in forests using 3D RT model simulations.

The objective of this study was to comprehensively assess VI saturation effects in forest scenes by combining satellite observations with a newly developed and well-validated 3D RT model – the large-scale remote sensing data and image simulation framework (LESS) (Qi et al., 2017, 2019), and examined the influence of environmental factors. The specific aims are to (1) compare the saturation phenomena of 36 VIs and understand the influence of soil brightness, distribution type and sun-sensor geometry based on simulation experiments, (2) develop quantitative metrics of saturation and provide a new perspective for analyzing saturation effect, and (3) evaluate the VI saturation property in temporal and spatial variability using satellite observations.

2. Data and methods

2.1. Vegetation indices

As the mathematical combination or transformation of reflectance in multi spectral channels, VIs are simple and effective dimensionless radiometric quantities developed to respond to the biophysical and biochemical properties of vegetation, while suppressing signals from other non-vegetation factors (Huete et al., 2002). In this study, 36 LAI-related VIs were selected for saturation evaluation, with 24 dual-band VIs (red-NIR) that are available to most modern satellite remote sensing instruments, 9 VIs incorporating blue or green bands, and 3 red-edge indices (see Table 1 for detailed descriptions, formulae, references). To better match the requirements of practical applications, all VIs listed are considered broad-band VIs. Narrow-band spectral indices are coerced to the closest broad-band spectrum. The bands and

Table 1
Definitions of the selected 36 vegetation indices.*

VIs	Description	Formula	Reference	Band used
ATSAVI	Adjusted Transformed Soil-Adjusted Vegetation Index	$\frac{a(\rho_{NIR}-a\rho_R-b)}{\rho_R+a\rho_{NIR}-ab+0.08(1+a^2)}$	(Baret, 1991)	['a', 'N', 'R', 'b']
AVI	Advanced Vegetation Index	$(\rho_{\mathrm{NIR}}(1-\rho_{\mathrm{R}})(\rho_{\mathrm{NIR}}-\rho_{\mathrm{R}}))^{\frac{1}{3}}$	(Rikimaru et al., 2002)	['N', 'R']
DVI	Difference Vegetation Index	$\rho_{NIR}-\rho_R$	(Roujean and Breon, 1995)	['N', 'R']
EVI	Enhanced Vegetation Index	$2.5\frac{\rho_{\mathrm{NIR}}-\rho_{\mathrm{R}}}{\rho_{\mathrm{NIR}}+6\rho_{\mathrm{R}}-7.5\rho_{\mathrm{B}}+1}$	(Huete et al., 1997)	['N', 'R','B']
EVI2	Two-Band Enhanced Vegetation Index	$2.5\frac{\rho_{\mathrm{NIR}}-\rho_{\mathrm{R}}}{\rho_{\mathrm{NIR}}+2.4\rho_{\mathrm{R}}+1}$	(Jiang et al., 2008)	['N', 'R']
ExGR	ExG - ExR Vegetation Index	$(2\rho_G-\rho_R-\rho_B)-(1.3\rho_R-\rho_G)$	(Meyer and Neto, 2008)	['G', 'R', 'B']
GARI	Green Atmospherically Resistant Vegetation Index	$\frac{\rho_{\mathrm{NIR}}-(\rho_G-\mathrm{gamma}\times(\rho_B-\rho_R))}{\rho_{\mathrm{NIR}}+(\rho_G+\mathrm{gamma}\times(\rho_B-\rho_R))}$	(Gitelson et al., 1996)	['N', 'G', "B", 'R','gamma"]
GEMI	Global Environment Monitoring Index	$\frac{2({\rho_{\mathrm{NIR}}}^2-{\rho_{\mathrm{R}}}^2)+1.5\rho_{\mathrm{NIR}}+0.5\rho_R}{\rho_{\mathrm{NIR}}+\rho_R+0.5}\left(1-0.25\frac{2({\rho_{\mathrm{NIR}}}^2-{\rho_{\mathrm{R}}}^2)+1.5\rho_{\mathrm{NIR}}+0.5\rho_R}{\rho_{\mathrm{NIR}}+\rho_R+0.5}-\frac{\rho_{\mathrm{R}}-0.125}{1-\rho_{\mathrm{R}}}\right.$	(Pinty and Verstraete, 1992)	['N', 'R']
IPVI	Infrared Percentage Vegetation Index	$\frac{\rho_{\mathrm{NIR}}}{\rho_{\mathrm{NIR}}+\rho_{\mathrm{R}}}$	(Crippen, 1990)	['N', 'R']
kNDVI	Kernel Normalized Difference Vegetation Index	$tanh(\mathrm{NDVI}^2)$	(Camps-Valls et al., 2021)	['N', 'R']
MNLI	Modified Non-Linear Vegetation Index	$\frac{(\rho_{NIR}^2-\rho_R)(1+L)}{(\rho_{NIR}^2+\rho_R+L)}$	(Gong et al., 2003)	['L', 'N', 'R']
MSAVI	Modified Soil-Adjusted Vegetation Index	$\frac{2\rho_{\mathrm{NIR}}+1-\sqrt{(2\rho_{\mathrm{NIR}}+1)^2-8(\rho_{\mathrm{NIR}}-\rho_{\mathrm{red}})}}{2}$	(Qi et al., 1994)	['N', 'R']
MSR	Modified Simple Ratio	$\frac{(\rho_{NIR}/\rho_R-1)}{\sqrt{\rho_{NIR}/\rho_R+1}}$	(Chen, 1996)	['N', 'R']
MSR705	Modified Simple Ratio (705 and 750 nm)	$\frac{(\rho_{750}/\rho_{705}-1)}{\sqrt{\rho_{750}/\rho_{705}+1}}$	(Wu et al., 2008)	['RE2', 'RE1']
MTVI1	Modified Triangular Vegetation Index 1	$1.2(1.2(\rho_{800}-\rho_{550})-2.5(\rho_{670}-\rho_{550}))$	(Haboudane et al., 2004)	['N', 'G', 'R']
NDVI	Normalized Difference Vegetation Index	$\frac{\rho_{\mathrm{NIR}}-\rho_{\mathrm{R}}}{\rho_{\mathrm{NIR}}+\rho_{\mathrm{R}}}$	(Rouse et al., 1974)	['N', 'R']
NDVI705 (NDVIre)	Normalized Difference Vegetation Index (705 and 750 nm)	$\frac{\rho_{750}-\rho_{705}}{\rho_{750}+\rho_{705}}$	(Sims and Gamon, 2002; Gitelson and Merzlyak, 1994)	['RE2', 'RE1']
NGRDI	Normalized Green Red Difference Index	$\frac{\rho_{\mathrm{G}}-\rho_{\mathrm{R}}}{\rho_{\mathrm{G}}+\rho_{\mathrm{R}}}$	(Tucker, 1979)	['G', 'R']
NIRv	Near-Infrared Reflectance of Vegetation	$\mathrm{NDVI}*\rho_{\mathrm{NIR}}$	(Badgley et al., 2017)	['N', 'R']
NLI	Non-Linear Vegetation Index	$\frac{{\rho_{\mathrm{NIR}}}^2-\rho_{\mathrm{R}}}{{\rho_{\mathrm{NIR}}}^2+\rho_{\mathrm{R}}}$	(Goel and Qin, 1994)	['N', 'R']
OSAVI	Optimized Soil-Adjusted Vegetation Index	$\frac{\rho_{\mathrm{NIR}}-\rho_{\mathrm{R}}}{\rho_{\mathrm{NIR}}+\rho_{\mathrm{R}}+0.16}$	(Rondeaux et al., 1996)	['N', 'R']
PVI	Perpendicular Vegetation Index	$\frac{\rho_{NIR}-a\rho_R-b}{\sqrt{a^2+1}}$	(Richardson and Wiegand, 1977; Jackson et al., 1980)	['N', 'R']
RCC	Red Chromatic Coordinate	$\frac{\rho_{\mathrm{R}}}{\rho_{\mathrm{R}}+\rho_{\mathrm{G}}+\rho_{\mathrm{B}}}$	(Gillespie et al., 1987)	['R', 'G', 'B']
RDVI	Renormalized Difference Vegetation Index	$\frac{\rho_{NIR}-\rho_R}{\sqrt{\rho_{NIR}+\rho_R}}$	(Roujean and Breon, 1995)	['N', 'R']
RGBVI	Red Green Blue Vegetation Index	$\frac{{\rho_G}^2-\rho_{\mathrm{B}}*\rho_{\mathrm{R}}}{{\rho_G}^2+\rho_{\mathrm{B}}*\rho_{\mathrm{R}}}$	(Bendig et al., 2015)	['G', 'B', 'R']
SAVI	Soil-Adjusted Vegetation Index	$\frac{(1+L)(\rho_{NIR}-\rho_R)}{\rho_{NIR}+\rho_R+L}$	(Huete, 1988)	['L', 'N', 'R']
SAVI2	Soil-Adjusted Vegetation Index 2	$\frac{\rho_{NIR}}{\rho_R+\mathrm{slb}/sla}$	(Major et al., 1990)	['N', 'R', 'b', 'a']
SR	Simple Ratio	$\frac{\rho_{NIR}}{\rho_R}$	(Jordan, 1969)	['N', 'R']
TDVI	Transformed Difference Vegetation Index	$1.5\frac{\rho_{NIR}-\rho_R}{\sqrt{{\rho_{\mathrm{NIR}}}^2+\rho_R+0.5}}$	(Bannari et al., 2002)	['N', 'R']
TGI	Triangular Greenness Index	$-0.5(190(\rho_{670}-\rho_{550})-120(\rho_{670}-\rho_{480}))$	(Hunt et al., 2013)	['R', 'G', 'B']
TriVI	Triangular Vegetation Index	$0.5(120(\rho_{NIR}-\rho_G)-200(\rho_R-\rho_G))$	(Broge and Leblanc, 2001)	['N', 'G', 'R']
TSAVI	Transformed Soil-Adjusted Vegetation Index	$\frac{a(\rho_{NIR}-a\rho_R-b)}{\rho_R+a\rho_{NIR}-ab}$	(Baret et al., 1989)	['a', 'N', 'R', 'b']
TVI	Transformed Vegetation Index	$\sqrt{\frac{\rho_{NIR}-\rho_R}{\rho_{NIR}+\rho_R}+0.5}$	(Rouse et al., 1974)	['N', 'R']
VI700	Vegetation Index (700 nm)	$(\rho_{700}-\rho_R)/(\rho_{700}+\rho_R)$	(Gitelson et al., 2002)	['RE1', 'R']
WDRVI	Wide Dynamic Range Vegetation Index	$(alpha\times\rho_{NIR}-\rho_R)/(alpha\times\rho_{NIR}+\rho_R)$	(Gitelson, 2004)	['alpha', 'N', 'R']
WDVI	Weighted Difference Vegetation Index	$\rho_{\mathrm{NIR}}-a\rho_{\mathrm{R}}$	(Clevers, 1989)	['N', 'a', 'R']

* 'B', 'G', 'R', and 'N' represent the blue, green, red, and NIR bands, respectively. 'RE1'and 'RE2' represent the red-edge 1 and red-edge 2 channels of Sentinel-2 Multispectral Instrument (MSI). a, b, and L are soil line parameters. a is the slope of the soil line and b is the intercept of the soil line with the NIR axis. The a values for dark, medium and bright soils are 1.0582, 0.6820 and 0.6493, respectively, and the b values for dark, medium and bright soils are 0.0877, 0.1793 and 0.1829, respectively. The L value is set to 0.5, as studies have demonstrated that L = 0.5 works well for SAVI in most situations and is generally used as the default value

(Nagy et al., 2018). *alpha* is the weighting coefficient used for WDRVI, which can range from 0.1 to 0.2. This study uses *alpha* value of 0.2, as recommended by (Gitelson, 2004). gamma is a weighting function that depends on aerosol conditions in the atmosphere and was set to 1.7 as recommended by (Gitelson et al. 1996).

parameters required for the VI computation are also listed in Table 1, and their selections were referred to (Montero et al., 2023).

2.2. Simulation experiments

The simulation experiments were designed to evaluate the different VI performances for forests and investigate the influence of several non-vegetation factors on the saturation effect, specifically the effects of different soil backgrounds, different distribution types (i.e., spatial distribution patterns of tree in a given geographic area), and different sun-sensor geometries, respectively. The specific experimental steps include spectral data acquisition, 3D forest scene construction, and multi-band bidirectional reflectance factors (BRFs) generation. The experimental procedure is presented in Fig. 1a.

We selected European white Birch, Scots Pine, Larix, and Eucalyptus (abbreviated as Birch, Pine, Larch, Eucalypt) as four representative species of deciduous broadleaf forest (DBF), evergreen needleleaf forest (ENF), deciduous needleleaf forest (DNF), and evergreen broadleaf forest (EBF), respectively. Spectral data for the components of individual trees were obtained from existing datasets (Elvidge, 1990; Hovi et al., 2021; Hovi et al., 2017; Juola et al., 2022; Lamsal et al., 2022; Noda et al., 2014; Rautiainen et al., 2022). The soil spectra were selected from the soil spectral library in ENVI software (https://www.ittvis.com/envi/). We sorted 25 soil spectral curves from low to high, taking the mean values of the first 10%, the middle 10%, and the last 10% as dark, medium, and bright soils. See Supplementary material Section 1.1 for details of the optical properties (leaves, barks, and soils) used.

In order to test the VI progressive changes in LAI increase, the LESS model version 2.0 (Qi et al., 2022) was used for 3D forest scenes construction and BRF generation with various combinations of vegetation types (four monocultures and two mixed forests), soil backgrounds (dark, medium, bright soils), distribution types (uniform distribution, "half-half" distribution, and row structure distribution), sun-sensor geometries (Solar Zenith Angle (SZA)/View Zenith Angle (VZA) were set to 0° to 70° with an interval of 10°, and Solar Azimuth Angle (SAA)/View Azimuth Angle (VAA) were set to 0° to 330° with an interval of 30°). The LAI of the simulated scenario varied from 0.25 to 7, with an interval of 0.25. The LESS model is a new ray-tracing-based 3D RT model, and its accuracy has been well validated using ground observations and other models (e.g., RAYTRAN, RAYSPREAD) from the RAMI website (https://rami-benchmark.jrc.ec.europa.eu/_www/index.php). As an effective and accurate tool for radiometric simulation over heterogeneous 3D scenes, LESS has recently become a popular and widely-used tool for remote sensing applications (Bian et al., 2021, 2022; Li and Mu, 2021; Yan et al., 2020). Detailed information about the LESS model can be found at Supplementary material Section 1.2, and details of the 3D forests construction and BRF simulations are provided in Supplementary material Section 1.3.

All simulations were performed at 2 nm intervals covering 400–900 nm, and then we combined the spectral response functions (SRFs) of the Sentinel-2 Multispectral Instrument (MSI) sensor with simulated continuous spectrum to calculate the broad-band reflectance based on Eq. S1. Finally, 36 VIs values for all scenes were computed according to the broadband reflectance and VI formulae.

2.3. Quantifying the saturation phenomenon based on simulations

The simulated data sets were used to compare the saturation properties of different VIs. Based on the characteristics of the VI-LAI scatter plot, we first constructed *VI* as the dependent variable of the continuous independent variable *LAI*. For comparison purposes, all VIs were normalized to obtain the same dynamic range by using the formula (Eq.

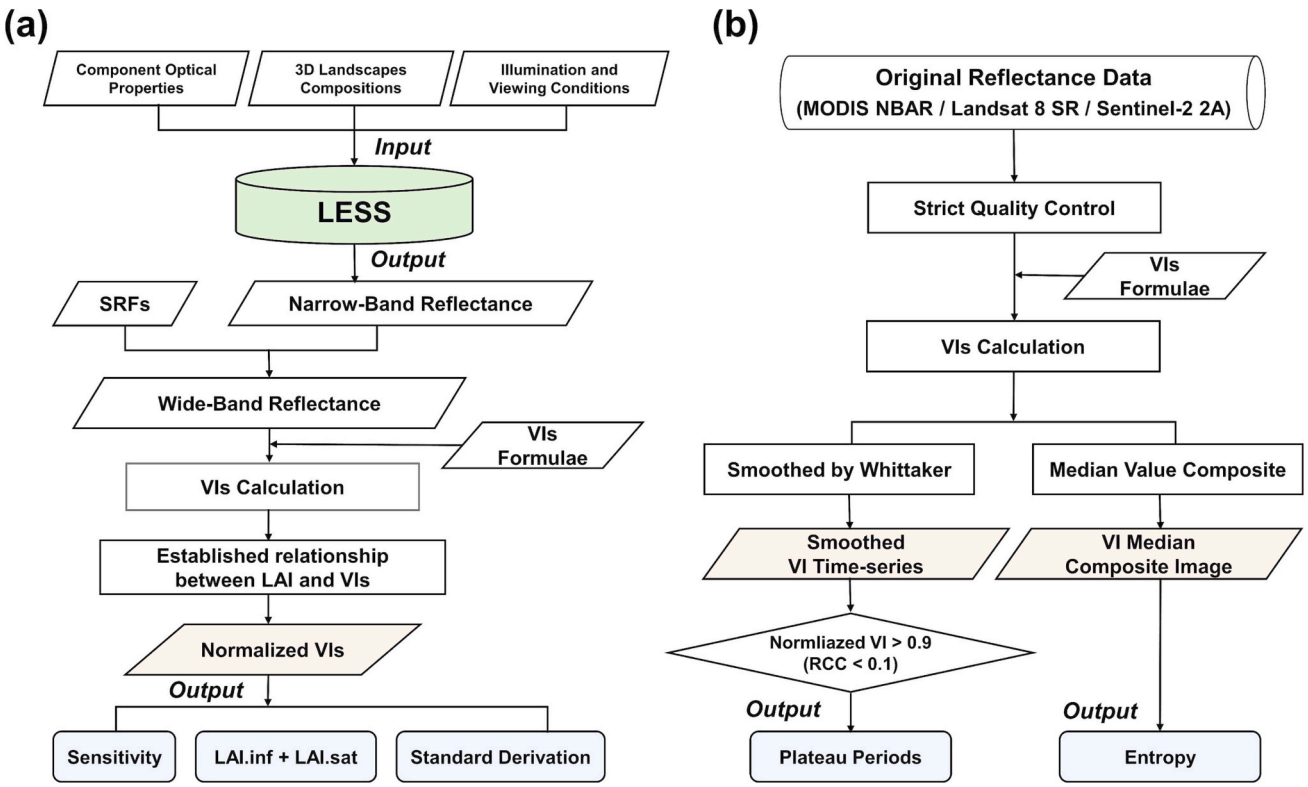

Fig. 1. Flowchart of the current study and the procedure of the (a) simulation experiments and (b) satellite experiments.

1). Sensitivity analysis will be conducted to assess changes in VI when varying different LAIs (Eq. 2). Meanwhile, the standard deviation (SD) of the normalized VIs was used to reflect the dispersion degree of the normalized VIs values for a set of LAIs, thus indirectly showing the ability of VIs to overcome saturation (Eq. 3). The larger the SD, the greater the dispersion of the VIs with LAI variation is, and the stronger the sensitivity of the VI is to the LAI.

$$VI_{normalized} = \frac{VI - VI_{min}}{VI_{max} - VI_{min}} \tag{1}$$

$$Sensitivity = \sqrt{\left(\frac{VI_i - VI_{i-1}}{LAI_i - LAI_{i-1}}\right)^2} \tag{2}$$

$$SD = \sqrt{\frac{1}{n}\sum_{i=1}^{n}(x_i - \bar{x})^2}, i = 1, 2, \ldots, n \tag{3}$$

where VI_{min} and VI_{max} are the maximum and minimum values of VIs in a set of 28 forest scenes with LAI from 0.25 to 7 with 0.25 interval; i represents the number of segments divided based on the same interval; x_i are the normalized VI values, $\bar{x}$ are the mean values of the normalized VIs.

In addition to these conventional methods, we have also proposed two indicators for assessing the VIs saturation effect related to LAI, namely the saturation inflection point (LAI.inf) and the saturation critical point (LAI.sat). The schematic description of the two metrics construction is in Fig. 2. Detailed definitions and calculations are summarized as follows.

2.3.1. Saturation inflection point – LAI.inf

Linear regression is widely used to estimate LAI from VIs for its simplicity (Zhen et al., 2021). When LAI increases to a certain value and no longer maintains a linear relationship with VIs, the saturation effect is observed. The purpose of the LAI.inf is to find the inflection point of the non-linear relationship between VI and LAI (Fig. 2c). According to the LAI.inf, the ground LAI range can be separated into two parts – unsaturated zone and saturated zone.

Based on the remarkable segmented trend between the VI–LAI response relationship, a two-piecewise linear regression model was used to determine LAI.inf (Harrell, 2015). For notational simplicity, we referred to LAI as x, VI as y, and LAI.inf as x_k.

$$y = \alpha + \beta_1 x_1 + \beta_2 x_2 + \varepsilon;\ \varepsilon \sim N(0, \sigma^2) \tag{4}$$

Where, x_1 and x_2 are two independent variables and $x_1 < x_2$, β_1 and β_1 denote the regression coefficients (i.e., slopes) of these two segments, and ε is a Gaussian random variable with expectation zero and variance σ^2. When $x < x_k$, $x_1 = x$, $x_2 = 0$; and when $x \geq x_k$, $x_1 = 0$, $x_2 = x$. If there is no significant difference between β_1 and β_1, Eq. (4) can be simplified as: $y = \alpha + \beta x + \varepsilon$. $x_k$that gives the two-piecewise linear regression model with the highest likelihood was identified using a two-step recurrence method, detailed as follows. Step 1 classifies the LAI range as increasing from 5% to 95% with an increment step of 5%, then uses them as the inflection points to perform segmented regressions and consequently find out which percentile points give the model the highest likelihood. The precise inflection point is narrowed down to ±4% percentile of the percentile points that give the highest likelihood among the 19 models. Step 2 continues the piecewise regression for three quartiles (25%, 50%,75%) in the ±4% range, and finally determines the precise inflection point - LAI.inf.

2.3.2. Saturation critical point – LAI.sat

In the later position of the saturated zone, LAI change was nearly not detectable using VIs. The purpose of the LAI.sat is to find the critical point that VIs cannot portray the surface LAI change after this (Fig. 2d).

The sensitivity curves of the VI for different LAIs were calculated based on Eq. 2. Then, due to the LAI constraints in our simulation experiments, the sensitivity <0.1 was chosen as the threshold below which VI changes are not acceptable for meaningful LAI characterization. LAI.sat is the corresponding LAI value when sensitivity equals 0.1.

Briefly, LAI.inf/LAI.sat can be simply understood as the onset/critical end of the saturation effect. The units of LAI.inf and LAI.sat were aligned to LAI (in the format $m^2 \bullet m^{-2}$).

2.4. Satellite experiments

The satellite experiments aim to test the VIs performance in a real-world application, and to verify the reliability of simulation results. To do so, we evaluated the behavior of VIs in terms of both spatial and temporal variability. A three-year time series of VIs was constructed based on reflectance datasets from Sentinel-2 MSI, Landsat 8 operational land imager (OLI), and moderate-resolution imaging spectroradiometer (MODIS) for the period January 1, 2019, to January 1, 2022, to assess

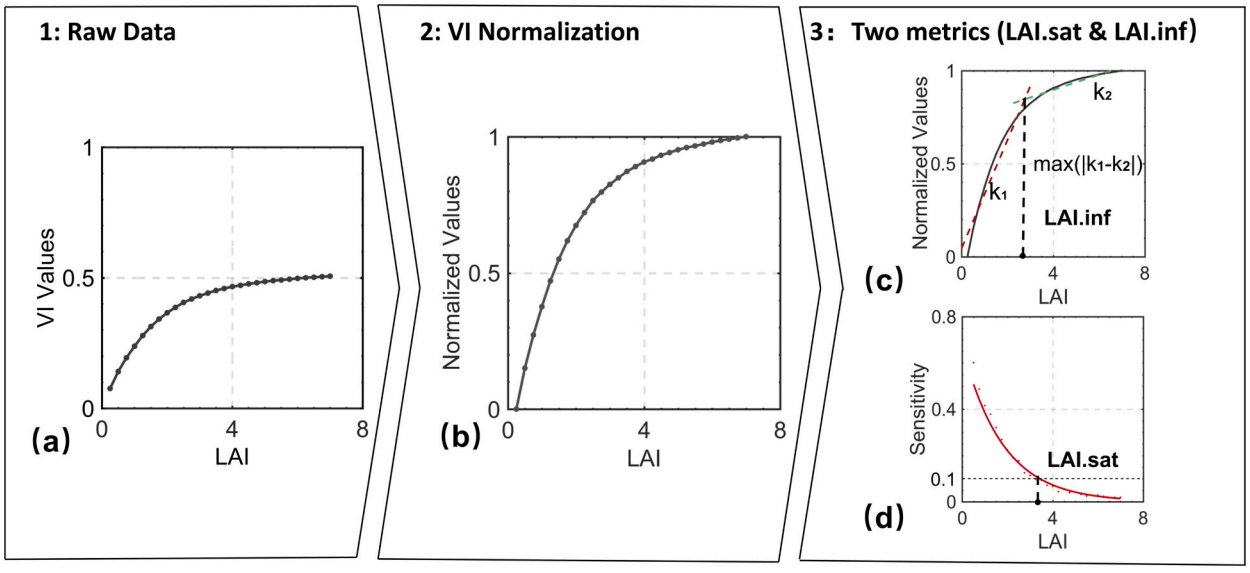

Fig. 2. Processing procedure. (a) VI acquired by the BRFs simulation in LESS; (b) VI normalization; Two indicators for the evaluation of the VI saturation phenomena, including (c) LAI saturation inflection point (LAI.inf) and (d) saturation critical point (LAI.sat).

the VIs' response to vegetation growth. To compare the ability of different VIs to characterize the spatial variability of vegetation, we randomly selected three different forest plots with high vegetation cover and evaluated the texture characteristics of the corresponding VI images derived from Sentinel-2 MSI data. Fig. 1b shows the workflow of the satellite experiments.

We restricted our analyses to areas with meaningful forest classes using these land cover products with matched - resolutions. Temporal analyses were conducted in the h12v04 tile as it has the highest coverage of DBF (Yan et al., 2021). Spatial variability analyses were carried out in three forest plots in the Amazon region, Canada, and China, which are highly vegetated regions and differ broadly in terms of vegetation composition, edaphic conditions, landform, and climate (details are provided in Supplementary material Section 2.1). The approximate locations of study areas on the world map are shown in Fig. 3.

The data process included quality control and smoothing continuous data. We centrally performed strict quality control for the reflectance data to identify erroneous data from the sensors and observation sources and minimize non-vegetative signals (i.e., clouds, clouds shadows, cirrus, snow). Since the three sensors onboard different platforms have different overpassing times, interpolation of the surface reflectance is required. Besides, the time series data often fluctuate abruptly due to seasonal impact and other noise in the satellite imagery. To compensate for this, the Whittaker smoothing algorithm was chosen for noise correction, which runs quickly but still balances the fidelity of noisy data with the smoothness of the resulting curve (Khanal et al., 2020). Details of satellite data Acquisition and processing can be found in Supplementary material Section 2.2.

2.5. Evaluation metrics for satellite observations

After quality control, VIs time series were calculated and normalized over each year's values to make an easy inter-comparison among different VIs. We set the plateau threshold at 0.9, and the period during which the normalized VI values exceeded this threshold (Normalized VI values >0.9) was taken as the plateau days. Note that the red chromatic coordinate (RCC) decreases with vegetation growth, so its threshold was set to 0.1, and days with normalized RCC <0.1 were used as plateau days. The plateau period comparison in different VIs provides a rough evaluation of the VI saturation effect in real satellite observations.

For spatial analysis, we employed the entropy of the VIs images as a statistical measure of randomness that can be used to characterize the VI image texture, and the related formula is as follows (Soh and Tsatsoulis, 1999):

$$Entropy = -\sum_{i=1}^{k} \frac{n_i}{N} \times log_2\left(\frac{n_i}{N}\right) \quad (5)$$

where N is the total number of observations, k is the number of classes in N, and n_i is the number of observations belonging to the same class.

3. Results

3.1. Sensitivity and saturation indicators of VIs to LAI for different forest scenes

Sensitivity is one of the most important indicators to evaluate the change of VI with LAI. The higher the sensitivity, the higher the accuracy of VI-based LAI retrieval. The normalized VIs and their sensitivity with LAI change for the Eucalypt monocultures under dark soil are presented in Fig. 4, and the remaining scenarios are shown in the Fig. S7. For all scenes, all indices show a non-linear relationship with LAI, except for the SR of Eucalyptus monocultures. The sensitivity of VI gradually decreased as the LAI increased and saturation occurred. SR was the most sensitive for all forest scenes. There were noticeable differences in VI performance between different forest scenes, with the smallest differences in Pine and the largest differences in Eucalypt.

To more intuitively compare the saturation property of VIs, we further calculated two saturation points (LAI.inf and LAI.sat) for each VI in six forest scenarios (Fig. 5), which indicate the LAI values corresponding to the onset (low cut-off LAI) and completion (high cut-off LAI) of VI saturation. The results show that Pine monocultures and mixed forests dominated by Pine appeared to be the most easily saturated, with lower LAI.inf (range 2.07–3.01) and LAI.sat (range 2.92–4.22) for all VIs. Conversely, another coniferous monoculture - Larch was less easily

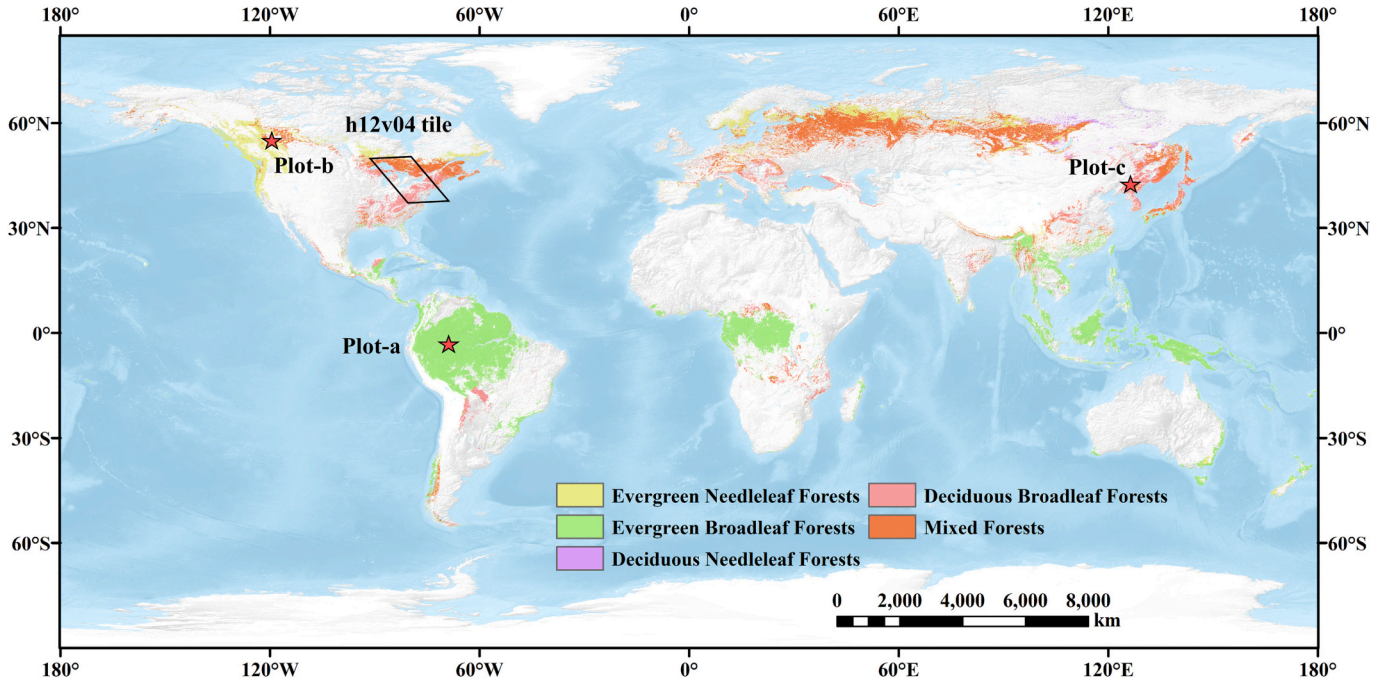

Fig. 3. Locations and land cover types of study areas (only forested areas are shown). The parallelogram circled is the study area used for temporal analysis. The locations marked with pentagons are the forest sample plots for spatial variability analysis, see Fig. S6 for further details.

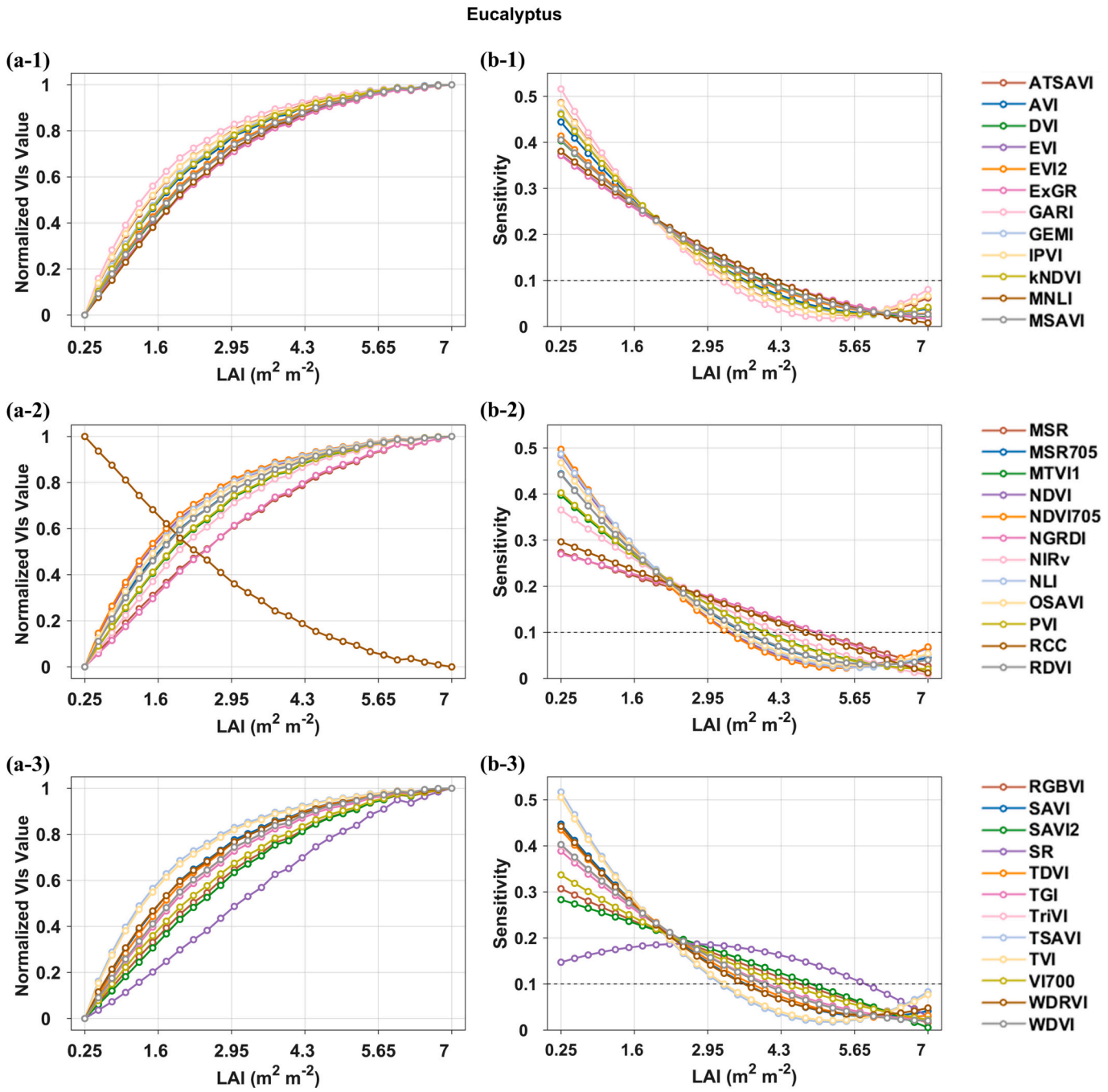

Fig. 4. The relationship between normalized VI values and VI sensitivities versus LAI for Eucalyptus monocultures under dark soil.

saturated, with the minimum LAI.inf and LAI.sat values at NDVI705, 3.26, and 3.8. The saturation points of mixed forests dominated by Pine were mostly located between Pine and Birch monocultures. The LAI.sat of mixed forests dominated by Birch was mostly higher than that of Birch monocultures, whereas LAI.inf was mostly smaller than that of Birch monocultures. Among the six forests, Eucalypt monocultures showed the largest differences in VI saturation points, where the largest extreme difference (maximum value – minimum value) in LAI.inf and LAI.sat could reach 1.64 and 2.99.

Hence, no definitive conclusions could be drawn from our results that VIs were more likely to saturate in coniferous or broad-leaved forests. This effectively means that the VI saturation effect was not well correlated to the species, but rather influenced by a combination of complex canopy structure and component optical properties. However, for all simulated forests, the ranking of the saturation resistance of these 336 VIs was mostly in agreement. Collectively, SR, RGBVI, NGRDI, MSR, and SAVI2 had the highest LAI.inf and LAI.sat value, followed by EVI, NIRv, MNLI, RCC, etc., and finally TVI, NDVI705, TSAVI, NDVI for all forests scenes.

3.2. *Influence of soil brightness*

We investigated the effect of soil varying in brightness as canopy understory on the saturation effect of different VIs. Fig. 6 shows histograms of the LAI.inf and LAI.sat values of VIs in six forest scenarios with three soil types. Among all indices, the SR performed best as having the highest LAI.inf and LAI.sat values, with mean values of 3.99 and 5.52 for all soil types and species, respectively. The saturation phenomena of SR,

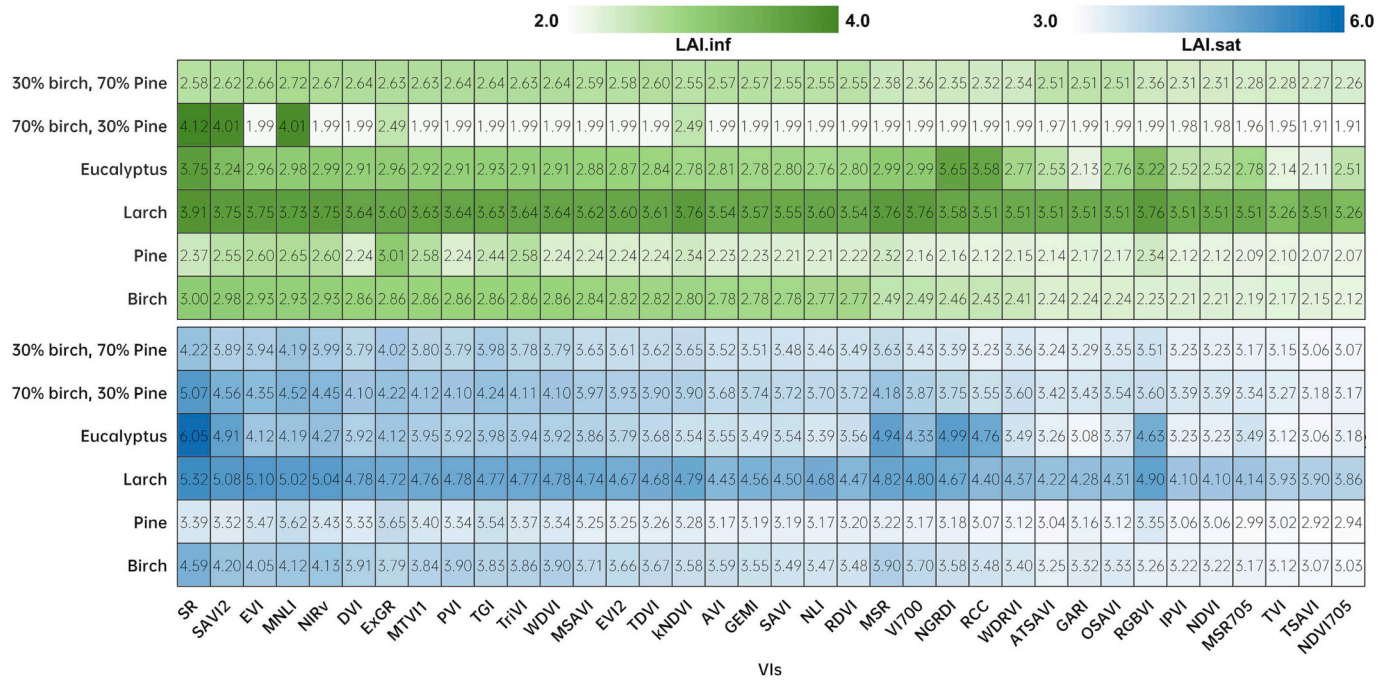

Fig. 5. LAI.inf and LAI.sat values in different VIs for six forests under dark soil. LAI.inf, saturation inflection points of VIs, means that a strong linear relationship can be observed between VIs and LAI before this value. LAI.sat, saturation critical points of VIs, means that VIs cannot portray the surface LAI change after this value. LAI.inf/LAI.sat can be simply understood as the onset/critical end of the saturation effect. The units of LAI.inf and LAI.sat were aligned to LAI (in the format $m^2 \bullet m^{-2}$).

ATSAVI, kNDVI, MSR, NGRDI, NLI, and RCC are very sensitive to soil brightness, especially in Larch monocultures, for example, the extreme differences of LAI.inf and LAI.sat of SR can almost reach 3. The saturation phenomena of AVI, DVI, MTVI1, MNLI, EXGR, TriVI, and PVI were less affected by soil. The saturation points of most VIs were increased with increasing soil brightness, while some VIs decreased with increasing soil brightness in Eucalyptus monocultures. In addition, we noted that EVI2, as an alternative to the EVI for sensors without the blue band, performed slightly worse than EVI, and both were less affected by soil brightness.

3.3. Influence of sun-sensor geometries

To study the influence of illumination and view geometry on the VI saturation, the SD of the normalized VIs (LAI range 0.25–7) was calculated for each angle combination. The performance of different VIs for 9216 angle combinations is depicted by box plots (Fig. 7). NLI, SR, RCC, kNDVI, MSR, NGRDI, and VI700 performed best (highlighted in orange color) collectively with high SD value (higher than 0.35) and were less affected by the sun-sensor geometry. TSAVI (highlighted in gray color) performed worst with median SD of 0.19 and highest interquartile range. WDVI, PVI, and SAVI2 (highlighted in purple color) demonstrated poor performance, with median SD of 0.19, 0.26, 0.29, and 0.29, respectively. Moreover, these four VIs were strongly influenced by angle, with extreme differences ranging from 0.15 to 0.23.

3.4. Variation among different vegetation distributions

We also investigated the saturation effect of VIs under different vegetation distributions, and the SD of normalized VIs with the solar position for Birch monocultures is shown in Fig. 8. Comparing the three distribution types, we found that the SD in the scene with uniform distribution was apparently higher and the difference was smaller at different solar angles. Even at the TSAVI with the greatest variation among different angles, the extreme difference of SD is only 0.18.

In the uniformly distributed vegetation scene, the SD of normalized VIs increased with SZA and does not change with changing SAA. In the forest scenarios with “half-half” distribution and row structure distribution, the SD of normalized VIs were centrally symmetric along the 90°-270°, and the variations in different solar positions were very pronounced in PVI and DVI. SAVI, EVI, EVI2, and NIRv revealed very similar characteristics, while SR, NGRDI, NLI, MSR, RCC, and kNDVI also showed a remarkably similar pattern. It is worth noting that the DVI performed differently in the forest scenes with uniform,”half-half”, and row structure distributions, with extreme differences of 0.02, 0.11, and 0.13, respectively. DVI showed higher SD mutation on the 0°-180° line for “half-half” distribution, and lower SD mutation on the 90°-270° line for row structure distribution.

3.5. Temporal and spatial variability of different VIs using satellite observations

Fig. 9 shows the mean plateau periods for 36 VIs from Sentinel - 2A MSI, Landsat 8 OLI, and MODIS data in 2019–2021. Most VIs from all three sensors had plateau periods <60 days per year, with the best performance being SR and the worst performance being TSAVI which could barely show vegetation dynamics (Fig. S9). The VIs of Sentinel-2A MSI and Landsat 8 OLI had better consistency in plateau period ranking, while MODIS does not agree with the other two sensors in the determination of the top-ranked VIs. TGI and EXG performed best in the MODIS data with average plateau periods of only 15 and 19 days, but are above 50 days for the other two sensors. This may be due to the fact that the spectral response to pixel components is different in different bands and sensors, thus complicating the VI behavior pattern. Moreover, it also reveals that the saturation properties of VI may not behave consistently at different spatial scales.

We further statistic the texture information of different normalized VIs computed from sentinel-2A MSI reflectance imagery for three forest plots. The probability density functions of the pixel statistics for each VIs image were fitted by the kernel density function, and the corresponding image entropy was calculated (Fig. 10). The image entropies of SR, MSR, NIRv, MSAVI, and SAVI2 were highest in all three forest plots. TVI, ExGR, and TVI clearly perform worse, and TSAVI performed the worst, with information entropy almost all equal to 0 and could not portray the

Fig. 6. The LAI.inf and LAI.sat in different VIs for six forests under dark soil, medium soil, and bright soil types. The green series is for LAI.inf, and the blue series is for LAI.sat. The color series from dark to light indicates dark soil, medium soil, and bright soil types. B, P, L, E, M1, and M2 are abbreviations for Birch, Pine, Larch, Eucalyptus monocultures, and mixed forest 1 and 2, respectively. (For interpretation of the references to color in this figure legend, the reader is referred to the web version of this article.)

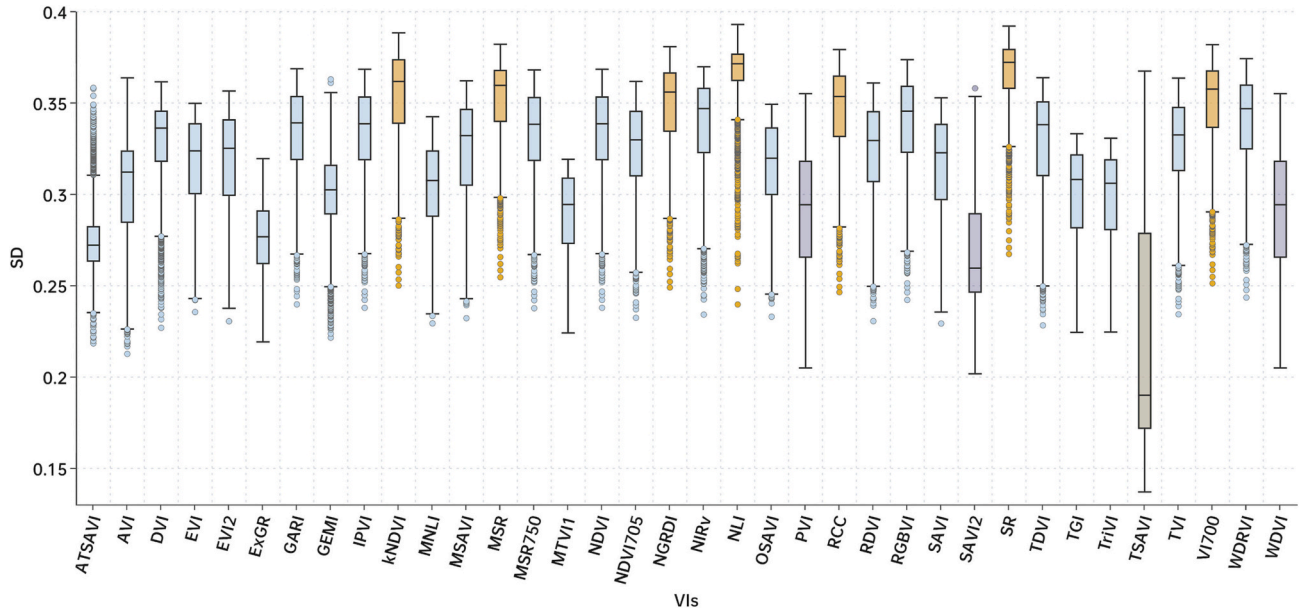

Fig. 7. Boxplots of the standard deviation of the normalized VIs for different combinations of solar and view angles. Solar zenith angle (SZA) and view zenith angle (VZA) were set to 0° to 70° with an interval of 10°, and solar azimuth angle (SAA) and view azimuth angle (VAA) were set to 0° to 330° with an interval of 30°, for a total of 9216 combinations. Boxes indicate the interquartile range with the median shown by horizontal lines, and individual points meaning outliers. The whiskers indicate the minimum and maximum value of data except for outliers. The normalized VIs values for all angle combinations are shown in the scatter plot Fig. S8.

surface information. In general, the information entropy ranking of VIs in all three plots is in reasonable agreement.

4. Discussion

4.1. VI saturation mechanism and influencing factors

VI saturation can be plausibly attributed to two factors: reflectance saturation and mathematical formulation, which has been discussed extensively in the literature (Gu et al., 2013; Liu et al., 2021; Mutanga et al., 2023; Zhao et al., 2012). In the case of NDVI, the chlorophyll absorbing red band quickly becomes insensitive with increasing vegetation canopy closure, while NIR band continuously increases due to multiple scattering effects. The imbalance between the slight decrease in the red reflectance and the continuous growth of NIR reflectance is transformed by the mathematical equation and ultimately determines that NDVI is prone to saturation.

Satellite-observed reflectance is the non-linear combination of vegetation, soil, shadows and other ground components, typically determined by leaf reflectance, soil reflectance, canopy structure and sun-sensor geometry (Qi et al., 2023). This also determines that the VI saturation can be influenced by these factors. First, the physiological characteristics of different tree species are quite different with different spectra of leaf, branch and bark components, which in turn leads to differences in VI saturation. For example, pine monoculture is most easily saturated because the leaf spectral of Pine has the least variation in red and NIR reflectance among all species. In addition, canopy structure (e.g., LAD, clumping index) affects VI saturation by influencing the radiative transfer process of photons through the canopy, as it determines how much incident light is multiply scattered, absorbed, and ultimately escapes from the canopy.

Soil background is also a key factor influencing the saturation effect of VIs. An interesting phenomenon was discovered in Section 3.2, bright soils are less likely to saturate for most indices, which may be explained by Fig. S7. Taking SR (NIR/Red) as an example, initially, the value of SR under dark soil is larger than that under bright soil in low vegetation cover; as the vegetation density increased, the contribution of vegetation in the canopy reflectance increases, but the SR of dark soil was still larger than that of bright soil; when the vegetation was fully covered, the soil did not contribute to the canopy reflectance, and finally all forests with different soil backgrounds all approach to the same SR value. It can also be inferred that the difference in SR saturation points in dark and medium soils should be greater than that in medium and bright soils (equal soil brightness intervals). In contrast, the saturation effect of DVI is hardly influenced by the soil background due to the fact that the slope of the soil spectra with different brightness are almost identical.

The sun-sensor geometry complicates the canopy reflectance observations and thus affects the VI saturation, mainly because the fraction of shadows in view changes as the relative positions of the sun and sensor change. We also found that ATSAVI, AVI, DVI, GEMI, PVI, SAVI2 and WDVI were negatively correlated with LAI at lower LAI levels (Fig. S8), which has been similarly reported in the literature (Zhen et al., 2021). This may result in an inaccurate estimation of the vegetation parameters. We speculated this is because that the soil component has higher reflectance in the NIR band than the vegetation component at some specific observation angles, leading to a decrease in NIR reflectance with increasing vegetation at lower LAI levels. VIs such as DVI and PVI, which are strongly contributed by NIR reflectance, may not increase strictly with increasing LAI, but first decreased and then increased. However, our conjecture remains to be further confirmed, which will be further investigated in future work.

4.2. Comprehensive ranking of VIs based on simulation and satellite results

Fig. 11a compares the saturation performance of the 36 selected VIs based on simulated results (LAI.inf and LAI.sat) and satellite results (entropy and plateau periods). The larger the saturation indicators, the higher the image entropy, and the smaller the plateau periods, the higher the ranking of the corresponding VIs in terms of saturation resistance. It was observed that the relative ranking of computational simulations and satellite results were mostly in fair agreement, especially for the top and bottom ranked VIs, which provides confidence in VI saturation evaluation based on 3D RT simulations. Overall, SR, SAVI2, MSR, and NIRv are least likely to saturate, while TSAVI, TVI, IPVI, NDVI, GARI, and ATSAVI show weaker resistance to saturation.

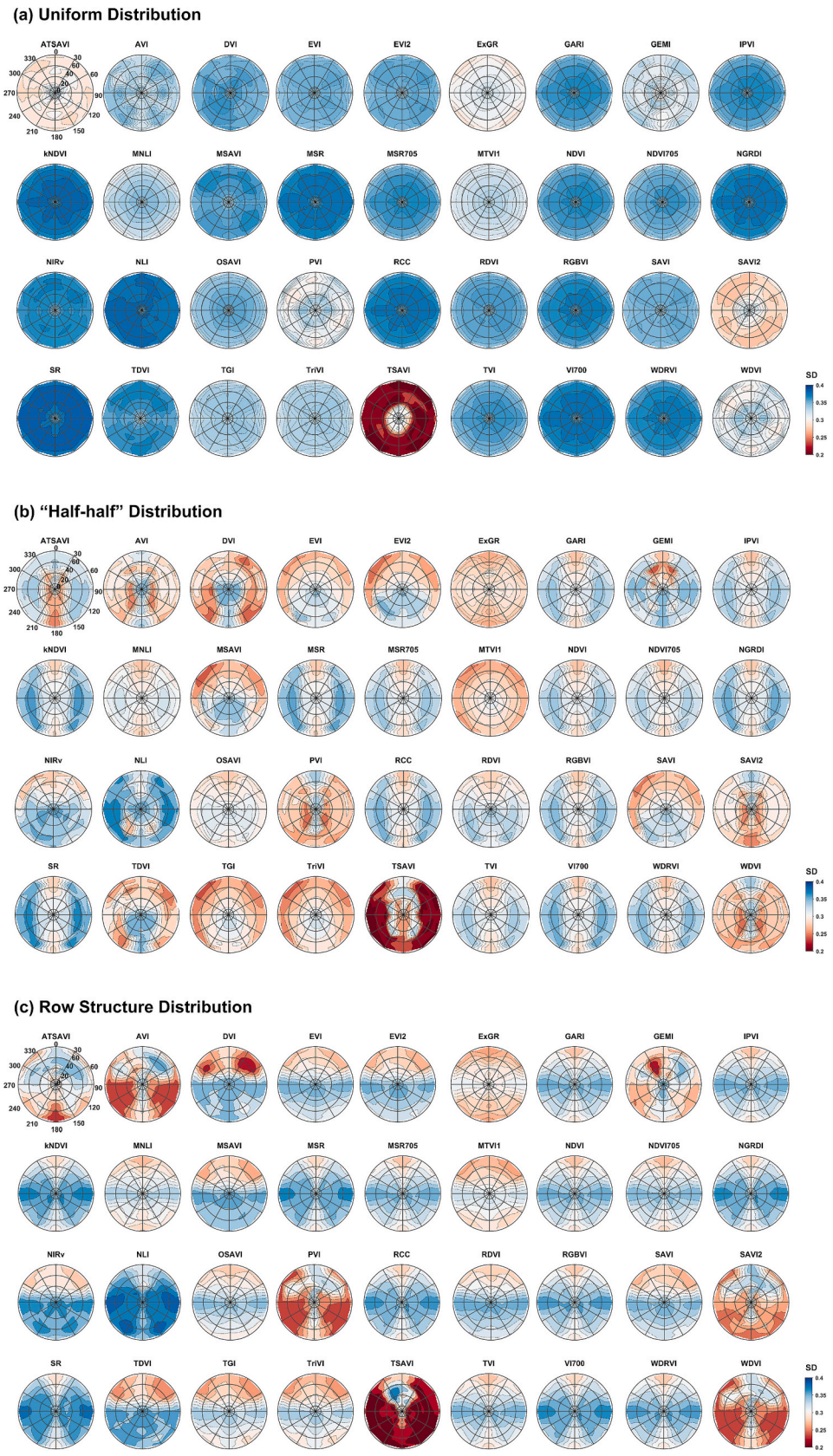

Fig. 8. Variations of standard deviation (SD) of the normalized VIs with the change of solar position for three vegetation distribution types (VZA = 0°, VAA = 0°). (a) Uniform distribution. (b) "Half-half distribution. (c) Row structure distribution.

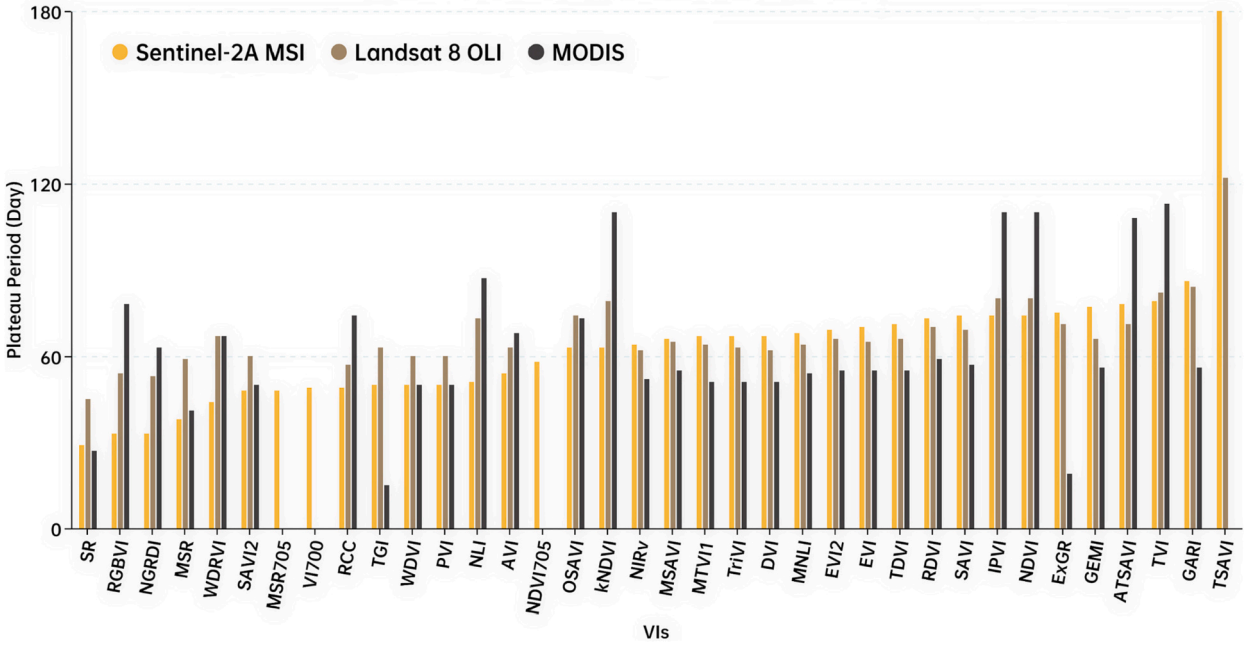

Fig. 9. Comparison of the mean plateau periods of the different VIs for Sentinel - 2A MSI, Landsat 8 OLI, and MODIS data in 2019–2021. The horizontal VIs are sorted from the minimum to the maximum value of the plateau periods for Sentinel-2A MSI, and the longer plateau period indicates that the VI is more likely to be saturated.

The upgraded VI - NDVI705 with the red edge band showed a slight improvement in saturation resistance over the original form - NDVI, while the MSR705 did not perform as well as the MSR. This reminds us that band introduction is not necessarily accompanied by an increased sensitivity of VI to vegetation changes, and that the mathematical form of VI is also a decisive factor.

Fig. 11b summarizes the ranking of the effects of VI saturation by non-vegetation factors, with higher rankings representing lower susceptibility to the factor. In contrast to Fig. 11a, we can find that most of the VIs with high resistance to saturation have a higher susceptibility to non-vegetation factors, such as NGRDI, SR, and MSR. Most of the indices were unable to balance the sensitivity to soil brightness, sun-sensor geometry, and distribution type. For example, PVI and WDVI exhibited better resistance to soil brightness but were sensitive to the angular effect. This finding is in line with the literature (Zeng et al., 2022). Overall, we found that MTVI1, MNLI, TGI, and TriVI performed the best, balancing high resistance to saturation and insensitivity to non-vegetation factors, both ranked in the first or second tier (Level 1 and Level 2). Despite some limitations of this internal comparison, our analytical approach reflects the advantage of 3D RT simulations, which are based on a strict single-variable principle and allow the separation of different variables for saturation evaluation. It is difficult to speculate on the sensitivity to various non-vegetation factors based on satellite observations alone.

4.3. Advantages and application of LAI.Sat and LAI.Inf

Reducing the saturation effect and increasing linearity would improve the accuracy of vegetation biophysical parameters estimation and increase confidence in the use of VIs (Huete et al., 2002; Jiang and Huete, 2010). Most studies on VI saturation evaluation were based on linear correlation (R^2) or mean sensitivity ($dVI/dLAI$), which provide a simple and straightforward description of VI performance over the entire LAI range to draw reliable conclusions (Aklilu Tesfaye and Gessesse Awoke, 2021; Huete et al., 1994). However, the saturation effect is indeed a gradual process, which is not only shown in our results (Fig. 6) but also widely discussed by the scientific community (Chang and Shoshany, 2016; Gitelson et al., 2002). In this case, the sensitivity and R^2 could only give an approximation rather than definite answers to the interesting phenomena in the saturation process, i.e., at what level of vegetation density VI starts to saturate, and at what level it is completely saturated.

Accordingly, this study defined the LAI.inf by piecewise linear regression and determined the LAI.sat by setting a sensitivity threshold, allowing for a better characterization of this gradual progress. LAI.inf captures the best performance range for VI linear detection of LAI, and LAI.sat reflects the limit of VI's ability to monitor surface LAI. According to the implications of these two indicators, the LAI range can be divided into three regions: well-characterized region (LAI < LAI.inf), vulnerable region (LAI.inf < LAI < LAI.sat), and saturation region (LAI > LAI.sat). The performances of VIs for Birch monocultures over dark soil are summarized in Fig. 12. As an example, the most widely used VI, NDVI, performed well at LAI < 2, but almost completely lost its ability to characterize vegetation when LAI > 3. The combination of LAI.sat and LAI.inf offers a more comprehensive description of the saturation effect and provides vital information for VI practical applications.

Based on the above considerations, we mapped the ability of NDVI to portray surface vegetation for EBF, ENF, DBF, DNF, and mixed forests based on our simulation results, and plotted the saturation ratios of MODIS LAI main algorithm (Fig. 13). The comparison between Fig. 13a and b reveals a noticeable consistency in the spatial distribution pattern of saturation effect between NDVI and MODIS LAI main algorithm, both of which easily saturate in tropical and subtropical regions at low latitudes. Note that the comparison here is only a rough approximation considering the saturation effect of VIs varies with space and species. The purposes of this comparison are to provide a global or regional perspective for the saturation effect, and also to alert researchers involved in vegetation monitoring to saturation phenomena and its spatial variation. Besides, our findings may inspire new formulations of the MODIS LAI backup algorithm. For instance, it might be more appropriate to determine VI according to actual ground state, like choosing SR, EVI, and NIRv that resist saturation better in densely forested areas, or using multiple VI combinations instead of only considering NDVI.

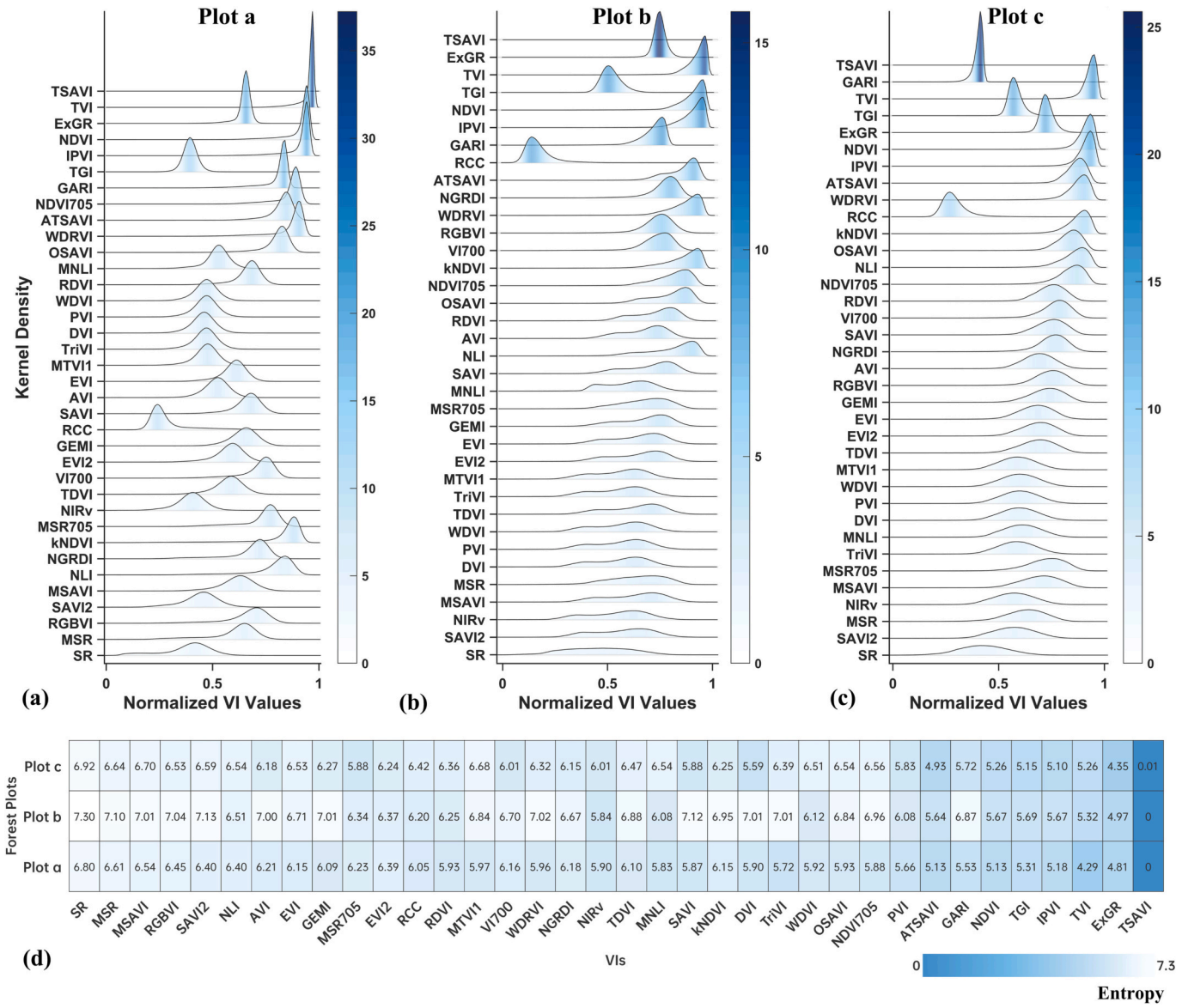

Fig. 10. Comparison of the spatial variability between the different VIs for Sentinel – 2A MSI images. (a-c) summary statistics of the texture information of the normalized VIs for the three forest plots. The solid curves represent the fitted kernel density estimates. Colors correspond to the density of the data points, with blue being the highest density and white being the lowest density. The vertical VI ranking is based on the value of image entropy. (d) Entropy value corresponding to plot a, b, and c. (For interpretation of the references to color in this figure legend, the reader is referred to the web version of this article.)

4.4. Implications for VI selection and application

In the present study, we conducted a comprehensive assessment of the VI saturation effect based on a combination of 3D RT simulations and satellite observations, considering the effects of different vegetation types, distribution types, soil brightness as well as sun-sensor geometries. However, a key question remains: which VI is most suitable for vegetation monitoring?

Indeed, saturation resistance is only one of the criteria when selecting VIs. The selection of the optimal VI should combine the ability to accurately portray vegetation and improve resistance to non-vegetation disturbances, rather than focusing exclusively on one or the other, as discussed in section 4.2. Furthermore, the choice of VI depends on user requirements since each VI has its strengths and limitations, and performs differently on different vegetation parameters estimation, e.g., kNDVI and NIRv have been shown as the accurate proxy to GPP despite it did not perform very well in our simulation studies (Badgley et al., 2017; Camps-Valls et al., 2021). As a next step, studies on VI saturation effects should be conducted for more vegetation parameters (e.g., Solar-induced chlorophyll fluorescence (SIF) (Braghiere et al., 2021)) in order to provide a wider range of VI options meeting a variety of user needs.

Finally, the scientific community should also be aware that even if suitable VIs are selected that can serve as a good representation of the vegetation biophysical properties over most regions and times, it is still not possible to avoid the signal saturation problem of optical remote sensing. It has been recognized in recent years that multi sensor fusion of observations can improve the time span, spatial and temporal resolution as well as the VIs' continuity (Veraverbeke et al., 2018). Similarly, it may be a promising strategy to improve the signal saturation problem of optical remote sensing. For example, LiDAR data can better take into account vertical structural parameters compared to optical remote sensing, thus improving signal saturation in high-density vegetation areas (Ehlers et al., 2022; Mutanga et al., 2023). To better avoid potential saturation problem, we suggest that future researchers could incorporate microwave and LiDAR data with VI to interpret the vegetation state in densely vegetated area.

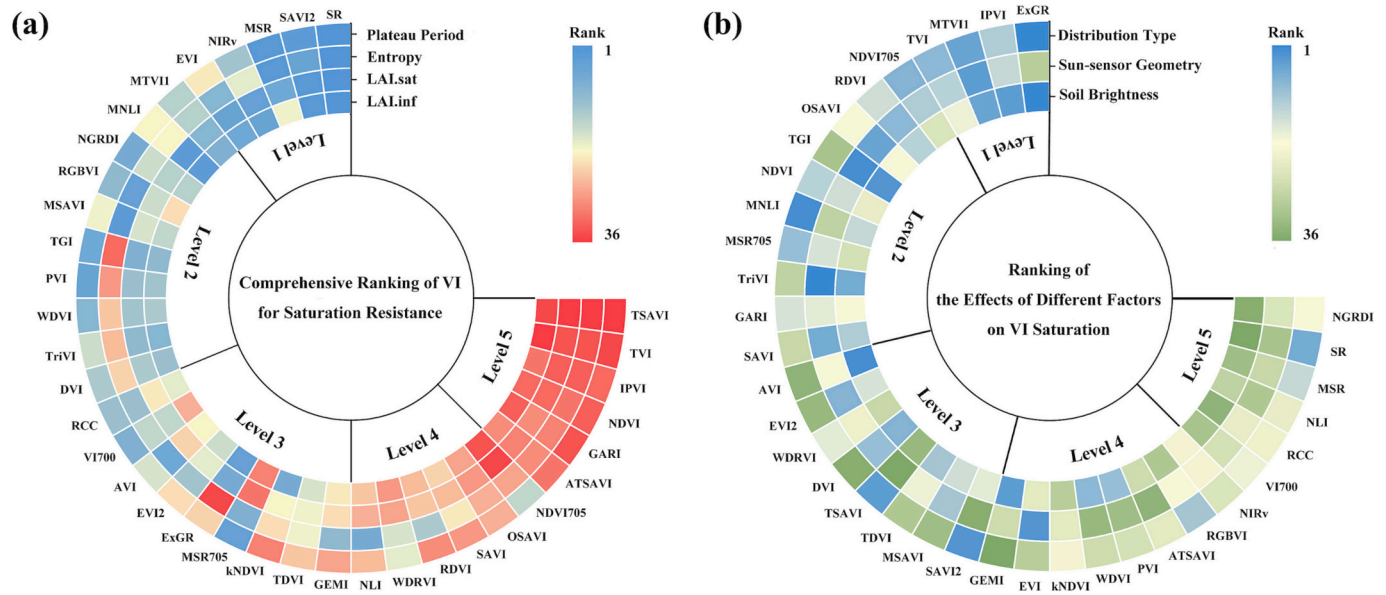

Fig. 11. A combined ranking of the 36 VIs' performance which was divided into five grades according to Jenks' natural break point classification method (Jenks, 1967). (a) Relative ranking of anti-saturation capability based on simulation results and satellite results. The higher the ranking, the higher the anti-saturation capability of the VIs. Level 1 to level 5: strong, relatively strong, moderate, relatively weak, and weak anti-saturation capacity, respectively. (b) Ranking of the effect of several non-vegetation factors on VI saturation based on the simulation result. Level 1 to level 5: strong, relatively strong, moderate, relatively weak, and weak resistance to disturbance factor, respectively.

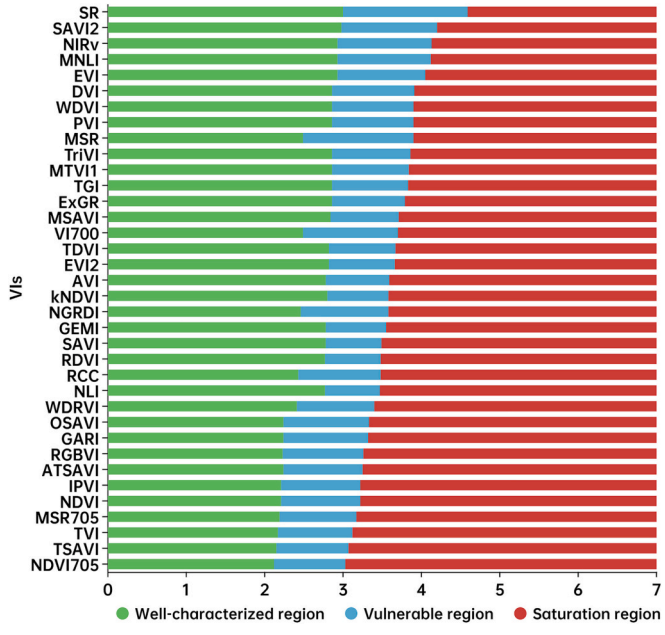

Fig. 12. Comparison of 36 VIs' ability in characterizing LAI for Birch monocultures under dark soil. The well-characterized region represents LAI < LAI.inf, the vulnerable region represents LAI.inf < LAI < LAI.sat, and the saturation region represents LAI > LAI.sat.

5. Conclusions

The saturation phenomenon that exists in vegetation indices (VIs) (greenness indicator) and leaf area index (LAI) (biomass indicator) cannot be avoided. Since the first vegetation index - SR was proposed in 1969, dozens of VIs and corresponding satellite products have been proposed in succession, providing a wealth of information on the status and changes of vegetation photosynthetic activity and canopy structure. However, the saturation effect poses a known limitation for the VIs application. Therefore, a careful assessment of saturation effects on different VIs is necessary to avoid the underestimation of biomass. This paper conducted a comprehensive evaluation of the VI saturation effect based on three-dimensional (3D) radiative transfer (RT) simulations and satellite observations, considering the effects of different vegetation types, distribution types, soil brightness as well as sun-sensor geometry. Two new metrics were proposed to describe the saturation effect in the simulation analyses from the application viewpoint. One is LAI.inf, which can limit the linear range of the relationship between VI and LAI and identifies the best ranges. The other indicator is LAI.sat, which limits the VI's ability to portray the surface LAI. The combination of these two metrics offers direct information for guiding the VI application.

Our study demonstrated that SR showed the best resistance to the saturation effect among the 36 VIs, followed by MSR, SAVI2, NIRv, EVI, etc., and finally TVI, IPVI, NDVI, GARI, ATSAVI, and TSAVI. The VIs saturation phenomenon behaved differently in different soil backgrounds, vegetation distributions, and sun-sensor geometry. The saturation effect of SR, NDVI, MSR and kNDVI were susceptible to soil brightness, while AVI, ATSAVI and PVI were easily influenced by angular effect. In addition, most of VIs were less prone to saturation and influenced by angular effect in uniformly distributed scenes than "half-half" and row structure distribution. The VIs' performance also varies between different satellite sensors and spatial scales, with the sentinel 2A MSI and landsat-8 OLI showing better agreement.

This study shed new light on the development of new VIs and selecting appropriate VIs for detecting vegetation biophysical parameters. There are many limitations associated with the current study. First, the simulated data are limited and we assessed vegetation index saturation only from the perspective of LAI changes. However, greenness is inherently a multidimensional and complex concept that requires the consideration of both qualitative (chlorophyll content) and quantitative (foliage cover, leaf area) effects, which may be interrelated and difficult to separate. In addition, the influence of topographic and scale effect on VI saturation have not been considered but warrant further investigation. The short-wave infrared indices have received considerable attention in recent years, but have not been considered in our study due to lack of spectral data. More ground measurements of component spectra and 3D realistic tree structures can support the simulation

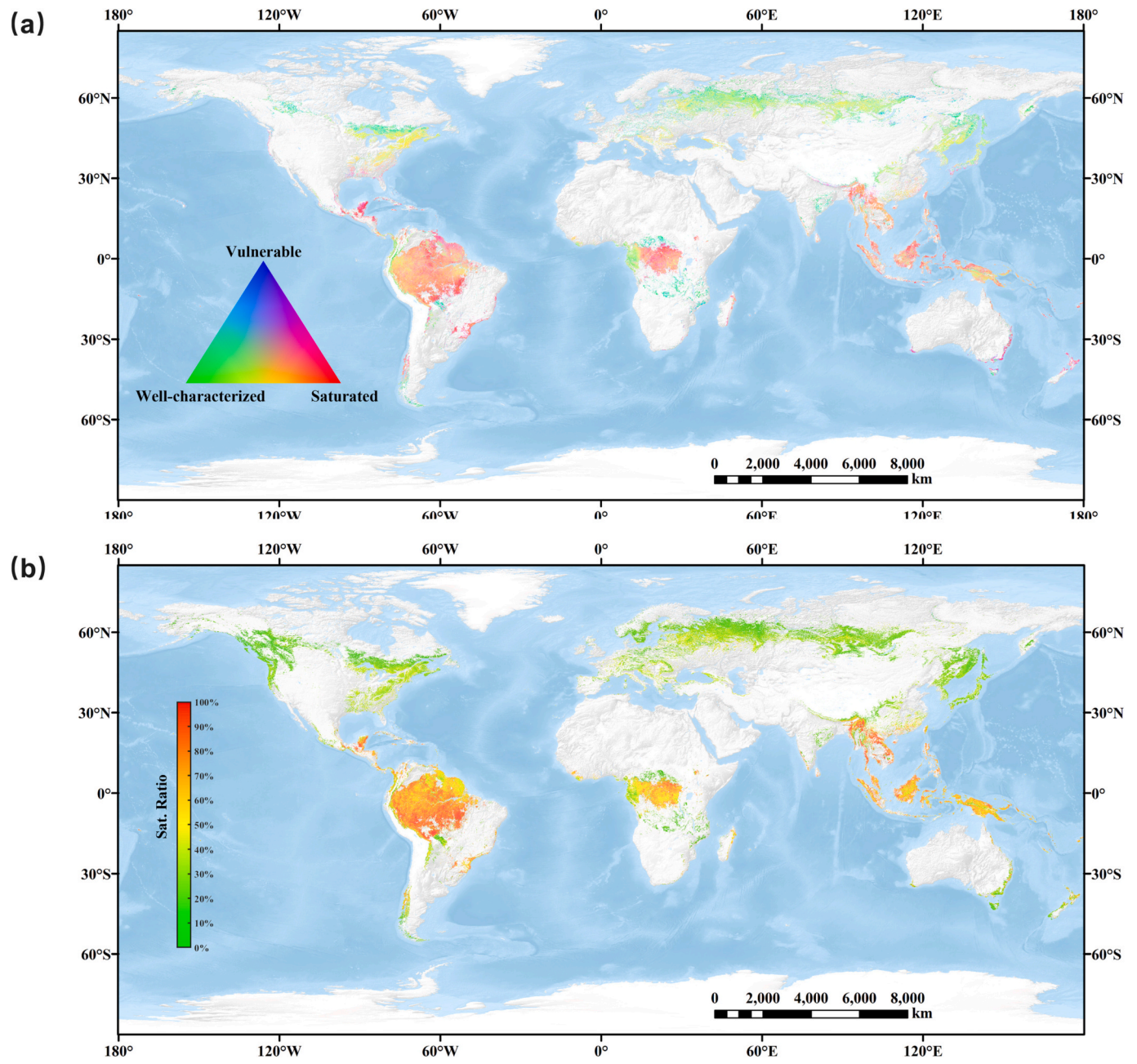

Fig. 13. (a) Ternary phase diagram of NDVI performance for global forests based on simulation results, where green indicates that NDVI can well characterize surface vegetation (LAI < LAI.inf), red denotes that NDVI saturation cannot characterize surface vegetation (LAI > LAI.sat), and blue represents vulnerable regions, i.e., buffer zones (LAI.inf < LAI < LAI.sat). (b) Ratio statistics of the saturated main MODIS LAI algorithm for global forests in 2019. Sat. The ratio indicates the proportion of days with a saturated main algorithm to the total number of days with the main algorithm in this pixel. (For interpretation of the references to color in this figure legend, the reader is referred to the web version of this article.)

experiments. In future research, we would continue to combine simulation experiments and satellite observations by consider these issues, and explore the relationships between more VIs and more vegetation physiological and biochemical parameters.

Credit author statement

Si Gao: Conceptualization, Methodology, Software, Writing - Original Draft, Visualization. Run Zhong: Conceptualization, Software. Kai Yan: Methodology, Writing - Review & Editing, Funding acquisition, Project administration. Jiabin Pu: Software and Investigation, Writing - Review & Editing. Xuanlong Ma: Methodology, Formal analysis and Evaluation, Funding acquisition. Xinkun Chen: Software and Investigation, Writing - Review & Editing. Jianbo Qi: Software and Methodology. Sicong Gao, Gaofei Yin: Editing, Methodology. Ranga B. Myneni: Conceptualization, Resources, Supervision.

Fundings

This work was supported in part by the National Natural Science Foundation of China Major Program (42192580) and the National Natural Science Foundation of China (42271356 and 42171305). (Corresponding authors: Kai Yan; Xuanlong Ma.)

Declaration of Competing Interest

The authors declare that they have no known competing financial interests or personal relationships that could have appeared to influence the work reported in this paper.

Data availability

Data will be made available on request.

Acknowledgments

The authors are very grateful to Miina Rautiainen for supporting spectral measurements. Constructive comments and recommendations by the editor and anonymous reviewers for improving the original manuscript are greatly appreciated. We would like to thank the high-performance computing support from the Center for Geodata and Analysis, Faculty of Geographical Science, Beijing Normal University [https://gda.bnu.edu.cn/].

Appendix A. Supplementary data

Supplementary data to this article can be found online at https://doi.org/10.1016/j.rse.2023.113665.

References

Aklilu Tesfaye, A., Gessesse Awoke, B., 2021. Evaluation of the saturation property of vegetation indices derived from sentinel-2 in mixed crop-forest ecosystem. Spat. Inf. Res. 29, 109–121. https://doi.org/10.1007/s41324-020-00339-5.

Badgley, G., Field, C.B., Berry, J.A., 2017. Canopy near-infrared reflectance and terrestrial photosynthesis. Sci. Adv. 3, 1–6. https://doi.org/10.1126/sciadv.1602244.

Baloloy, A.B., Blanco, A.C., Candido, C.G., Argamosa, R.J.L., Dumalag, J.B.L.C., Dimapilis, L.L.C., Paringit, E.C., 2018. Estimation of mangrove forest aboveground biomass using multispectral bands, vegetation indices and biophysical variables derived from optical satellite imageries: rapideye, planetscope and sentinel-2. ISPRS Ann. Photogramm. Remote Sens. Spat. Inform. Sci. 29–36.

Bannari, A., Asalhi, H., Teillet, P.M., 2002. Transformed difference vegetation index (TDVI) for vegetation cover mapping. Int. Geosci. Remote Sens. Symp. 5, 3053–3055. https://doi.org/10.1109/igarss.2002.1026867.

Baret, F., 1991. Potentials and limits of vegetation indices for LAI and APAR assessment. Remote Sens. Environ. 16, 161–173. https://doi.org/10.2136/sssaj1977.03615995004100040037x.

Baret, F., Guyot, G., Major, D.J., 1989. TSAVI: a vegetation index which minimizes soil brightness effects on LAI and APAR estimation. In 12th Canadian Symp. on Remote Sensing and IGARSS'90, Vancouver, Canada, 10-14 July 1989.

Bendig, J., Yu, K., Aasen, H., Bolten, A., Bennertz, S., Broscheit, J., Gnyp, M.L., Bareth, G., 2015. Combining UAV-based plant height from crop surface models, visible, and near infrared vegetation indices for biomass monitoring in barley. Int. J. Appl. Earth Obs. Geoinf. 39, 79–87. https://doi.org/10.1016/j.jag.2015.02.012.

Bian, Z., Roujean, J.-L., Cao, B., Du, Y., Li, H., Gamet, P., Fang, J., Xiao, Q., Liu, Q., 2021. Modeling the directional anisotropy of fine-scale TIR emissions over tree and crop canopies based on UAV measurements. Remote Sens. Environ. 252, 112150 https://doi.org/10.1016/j.rse.2020.112150.

Bian, Z., Wu, S., Roujean, J.-L., Cao, B., Li, H., Yin, G., Du, Y., Xiao, Q., Liu, Q., 2022. A TIR forest reflectance and transmittance (FRT) model for directional temperatures with structural and thermal stratification. Remote Sens. Environ. 268, 112749 https://doi.org/10.1016/j.rse.2021.112749.

Braghiere, R.K., Quaife, T., Black, E., He, L., Chen, J.M., 2019. Underestimation of global photosynthesis in Earth System models due to representation of vegetation structure. Glob. Biogeochem. Cycles 33, 1358–1369. https://doi.org/10.1029/2018GB006135.

Braghiere, R.K., Wang, Y., Doughty, R., Sousa, D., Magney, T., Widlowski, J.-L., Longo, M., Bloom, A.A., Worden, J., Gentine, P., Frankenberg, C., 2021. Accounting for canopy structure improves hyperspectral radiative transfer and sun-induced chlorophyll fluorescence representations in a new generation Earth System model. Remote Sens. Environ. 261, 112497 https://doi.org/10.1016/j.rse.2021.112497.

Broge, N.H., Leblanc, E., 2001. Comparing prediction power and stability of broadband and hyperspectral vegetation indices for estimation of green leaf area index and canopy chlorophyll density. Remote Sens. Environ. 76, 156–172. https://doi.org/10.1016/S0034-4257(00)00197-8.

Camps-Valls, G., Campos-Taberner, M., Moreno-Martínez, Á., Walther, S., Duveiller, G., Cescatti, A., Mahecha, M.D., Muñoz-Marí, J., García-Haro, F.J., Guanter, L., Jung, M., Gamon, J.A., Reichstein, M., Running, S.W., 2021. A unified vegetation index for quantifying the terrestrial biosphere. Sci. Adv. 7 https://doi.org/10.1126/sciadv.abc7447.

Cao, Z., Cheng, T., Ma, X., Tian, Y., Zhu, Y., Yao, X., Chen, Q., Liu, S., Guo, Z., Zhen, Q., Li, X., 2017. A new three-band spectral index for mitigating the saturation in the estimation of leaf area index in wheat. Int. J. Remote Sens. 38, 3865–3885. https://doi.org/10.1080/01431161.2017.1306141.

Carlson, T.N., Ripley, D.A.J., 1997. On the relation between NDVI, fractional vegetation cover, and leaf area index. Remote Sens. Environ. 62, 241–252.

Chang, J., Shoshany, M., 2016. Red-edge ratio Normalized Vegetation Index for remote estimation of green biomass. Int. Geosci. Remote Sens. Symp. (IGARSS) 1337–1339. https://doi.org/10.1109/IGARSS.2016.7729340.

Chen, J.M., 1996. Evaluation of vegetation indices and a modified simple ratio for boreal applications. Can. J. Remote Sens. 22, 229–242. https://doi.org/10.1080/07038992.1996.10855178.

Clevers, J., 1989. Application of a weighted infrared-red vegetation index for estimating leaf Area Index by Correcting for Soil Moisture. Remote Sens. Environ. 29, 25–37. https://doi.org/10.1016/0034-4257(89)90076-X.

Crippen, R.E., 1990. Calculating the vegetation index faster. Remote Sens. Environ. 34, 71–73. https://doi.org/10.1016/0034-4257(90)90085-Z.

Ehlers, D., Wang, C., Coulston, J., Zhang, Y., Pavelsky, T., Frankenberg, E., Woodcock, C., Song, C., 2022. Mapping forest aboveground biomass using multisource remotely sensed data. Remote Sens. 14 https://doi.org/10.3390/rs14051115.

Elvidge, C.D., 1990. Visible and near infrared reflectance characteristics of dry plant materials. Int. J. Remote Sens. 11, 1775–1795. https://doi.org/10.1080/01431169008955129.

Etchegorry, J.P.G., Yin, T., Lauret, N., Cajgfinger, T., Gregoire, T.G., Grau, E., Féret, J.-B., Lopes, M., Guilleux, J., Dedieu, G., Malenovsky, Z., Cook, B.D., Morton, D.C., Rubio, J., Durrieu, S., Cazanave, G., Martin, E., Ristorcelli, T., 2015. Discrete Anisotropic Radiative Transfer (DART 5) for modeling airborne and satellite spectroradiometer and LIDAR acquisitions of natural and urban landscapes. Remote Sens 7, 1667–1701.

Fang, H., Liang, S., 2003. Retrieving leaf area index with a neural network method: simulation and validation. IEEE Trans. Geosci. Remote Sens. 41, 2052–2062. https://doi.org/10.1109/TGRS.2003.813493.

Gamon, J.A., Penuelas, J., Field, C.B., 1992. A narrow-waveband spectral index that tracks diurnal changes in photosynthetic efficiency. Remote Sens. Environ. 41, 35–44. https://doi.org/10.1016/0034-4257(92)90059-S.

Gamon, J.A., Huemmrich, K.F., Wong, C.Y.S., Ensminger, I., Garrity, S., Hollinger, D.Y., Noormets, A., Peñuelask, J., 2016. A remotely sensed pigment index reveals photosynthetic phenology in evergreen conifers. Proc. Natl. Acad. Sci. U. S. A. 113, 13087–13092. https://doi.org/10.1073/pnas.1606162113.

Gao, X., Huete, A.R., Ni, W., Miura, T., 2000. Optical-biophysical relationships of vegetation spectra without background contamination. Remote Sens. Environ. 74, 609–620. https://doi.org/10.1016/S0034-4257(00)00150-4.

Gao, L., Wang, X., Johnson, B.A., Tian, Q., Wang, Y., Verrelst, J., Mu, X., Gu, X., 2020. Remote sensing algorithms for estimation of fractional vegetation cover using pure vegetation index values: a review. ISPRS J. Photogramm. Remote Sens. 159, 364–377.

Gillespie, A.R., Kahle, A.B., Walker, R.E., 1987. Color enhancement of highly correlated images. II. Channel ratio and "chromaticity" transformation techniques. Remote Sens. Environ. 22, 343–365. https://doi.org/10.1016/0034-4257(87)90088-5.

Gitelson, A., 2004. Wide dynamic range vegetation index for remote quantification of biophysical characteristics of vegetation. J. Plant Physiol. 161, 165–173. https://doi.org/10.1078/0176-1617-01176.

Gitelson, A., Merzlyak, M.N., 1994. Spectral reflectance changes associated with autumn senescence of Aesculus hippocastanum L. and Acer platanoides L. leaves. Spectral features and relation to chlorophyll estimation. J. Plant Physiol. 143, 286–292. https://doi.org/10.1016/S0176-1617(11)81633-0.

Gitelson, A., Kaufman, Y.J., Merzlyak, M.N., 1996. Use of a green channel in remote sensing of global vegetation from EOS-MODIS. Remote Sens. Environ 58, 289–298. https://doi.org/10.1016/S0034-4257(96)00072-7.

Gitelson, A., Kaufman, Y.J., Stark, R., Rundquist, D., 2002. Novel algorithms for remote estimation of vegetation fraction. Remote Sens. Environ. 80, 76–87. https://doi.org/10.1016/S0034-4257(01)00289-9.

Glenn, E., Huete, A., Nagler, P., Nelson, S., 2008. Relationship between remotely-sensed vegetation indices, canopy attributes and plant physiological processes: what vegetation indices can and cannot tell us about the landscape. Sensors 8, 2136–2160. https://doi.org/10.3390/s8042136.

Goel, N., Qin, W., 1994. Influences of canopy architecture on relationships between various vegetation indices and LAI and FPAR: a computer simulation. Remote Sens. Rev. 10, 309–347. https://doi.org/10.1080/02757259409532252.

Gong, P., Pu, R., Biging, G.S., Larrieu, M.R., 2003. Estimation of forest leaf area index using vegetation indices derived from Hyperion hyperspectral data. IEEE Trans. Geosci. Remote Sens. 41, 1355–1362.

Gu, Y., Wylie, B., Howard, D., Phuyal, K., Ji, L., 2013. NDVI saturation adjustment: a new approach for improving cropland performance estimates in the Greater Platte River Basin, USA. Ecol. Indic. 30, 1–6. https://doi.org/10.1016/j.ecolind.2013.01.041.

Haboudane, D., Miller, J.R., Pattey, E., Zarco-Tejada, P.J., Strachan, I.B., 2004. Hyperspectral vegetation indices and novel algorithms for predicting green LAI of crop canopies: Modeling and validation in the context of precision agriculture. Remote Sens. Environ. 90, 337–352. https://doi.org/10.1016/j.rse.2003.12.013.

Harrell, F., 2015. Regression Modeling Strategies, Springer Series in Statistics. Springer International Publishing, Cham. https://doi.org/10.1007/978-3-319-19425-7.

Hovi, A., Forsström, P.R., Ghielmetti, G., Schaepman, M.E., Rautiainen, M., 2021. A dataset composed of multiangular spectral libraries and auxiliary data at tree, leaf, needle, and bark level for three common European tree species. Data in Brief 35, 106820.

Hovi, A., Raitio, P., Rautiainen, M., 2017. A spectral analysis of 25 boreal tree species. Silva Fennica 51. https://doi.org/10.14214/sf.7753.

Huang, C., Yang, Q., Guo, Y., Zhang, Y., Guo, L., 2020. The pattern, change and driven factors of vegetation cover in the Qin Mountains region. Sci. Rep. 10, 20591.
Huete, A., Justice, C., Liu, H., 1994. Development of vegetation and soil indices for MODIS-EOS. Remote Sens. Environ. 49, 224–234. https://doi.org/10.1016/0034-4257(94)90018-3.
Huete, A., Liu, Q., van Leeuwen, W.J.D., 1997. Use of vegetation indices in forested regions: issues of linearity and saturation. Int. Geosci. Remote Sens. Symp. (IGARSS) 4, 1966–1968. https://doi.org/10.1109/igarss.1997.609169.
Huete, A., 1988. A soil-adjusted vegetation index (SAVI). Remote Sens. Environ. 25, 295–309.
Huete, A., Didan, K., Miura, T., Rodriguez, E., Gao, X., Ferreira, L., 2002. Overview of the radiometric and biophysical performance of the MODIS vegetation indices. Remote Sens. Environ. 83, 195–213. https://doi.org/10.1016/S0034-4257(02)00096-2.
Hunt, E.R., Doraiswamy, P.C., McMurtrey, J.E., Daughtry, C.S.T., Perry, E.M., Akhmedov, B., 2013. A visible band index for remote sensing leaf chlorophyll content at the Canopy scale. Int. J. Appl. Earth Obs. Geoinf. 21, 103–112. https://doi.org/10.1016/j.jag.2012.07.020.
Jackson, R.D., Pinter Jr., P.J., Reginato, R.J., Idso, S.B., 1980. Hand-held radiometry: a set of notes developed for use at the workshop of hand-held radiometry.
Jenks, G.F., 1967. The data model concept in statistical mapping. Int. Yearb. Cartogr. 7, 186–190.
Jiang, Z., Huete, A., 2010. Linearization of NDVI based on its relationship with vegetation fraction. Photogramm. Eng. Remote. Sens. 76, 965–975. https://doi.org/10.14358/PERS.76.8.965.
Jiang, Z., Huete, A., Li, J., Chen, Y., 2006. An analysis of angle-based with ratio-based vegetation indices. IEEE Trans. Geosci. Remote Sens. 44, 2506–2513. https://doi.org/10.1109/TGRS.2006.873205.
Jiang, Z., Huete, A.R., Didan, K., Miura, T., 2008. Development of a two-band enhanced vegetation index without a blue band. Remote Sens. Environ. 112, 3833–3845. https://doi.org/10.1016/j.rse.2008.06.006.
Jin, H., Eklundh, L., 2014. A physically based vegetation index for improved monitoring of plant phenology. Remote Sens. Environ. 152, 512–525. https://doi.org/10.1016/j.rse.2014.07.010.
Jordan, C.F., 1969. Derivation of Leaf-Area Index from Quality of Light on the Forest Floor. Ecol. Soc. Am. 50, 663–666. https://doi.org/10.2307/1936256.
Juola, J., Hovi, A., Rautiainen, M., 2022. A dataset of stem bark reflectance spectra for boreal and temperate tree species. Mendeley Data V2. https://doi.org/10.17632/pwfxgzz5fj.2.
Kerr, J., Ostrovsky, M., 2003. From space to species: ecological applications for remote sensing. Trends Ecol. Evol. 18, 299–305.
Khanal, N., Matin, M., Uddin, K., Poortinga, A., Chishtie, F., Tenneson, K., Saah, D., 2020. A comparison of three temporal smoothing algorithms to improve land cover classification: a case study from NEPAL. Remote Sens. 12, 5–7. https://doi.org/10.3390/RS12182888.
Kobayashi, H., Iwabuchi, H., 2008. A coupled 1-D atmosphere and 3-D canopy radiative transfer model for canopy reflectance, light environment, and photosynthesis simulation in a heterogeneous landscape. Remote Sens. Environ. 112, 173–185.
Kobayashi, H., Baldocchi, D., Ryu, Y., Chen, Q., Ma, S., Osuna, J., Ustin, S., 2012. Modeling energy and carbon fluxes in a heterogeneous oak woodland: a three-dimensional approach. Agric. For. Meteorol. 152, 83–100. https://doi.org/10.1016/j.agrformet.2011.09.008.
Köhler, P., Guanter, L., Kobayashi, H., Walther, S., Yang, W., 2018. Assessing the potential of sun-induced fluorescence and the canopy scattering coefficient to track large-scale vegetation dynamics in Amazon forests. Remote Sens. Environ. 204, 769–785. https://doi.org/10.1016/j.rse.2017.09.025.
Lamsal, K., Malenovský, Z., Woodgate, W., Waterman, M., Brodribb, T.J., Aryal, J., 2022. Spectral retrieval of eucalypt leaf biochemical traits by inversion of the Fluspect-Cx Model. Remote Sens. 14, 567. https://doi.org/10.3390/rs14030567.
Leigh, E.G., 1999. Tropical Forest Ecology: A View from Barro Colorado Island.
Li, W., Mu, X., 2021. Using fractal dimension to correct clumping effect in leaf area index measurement by digital cover photography. Agric. For. Meteorol. 311, 108695 https://doi.org/10.1016/j.agrformet.2021.108695.
Liu, Y., Qian, J., Yue, H., 2021. Comparison and evaluation of different dryness indices based on vegetation indices-land surface temperature/albedo feature space. Adv. Space Res. 68, 2791–2803. https://doi.org/10.1016/j.asr.2021.05.007.
Ma, X., Huete, A., Yu, Q., Restrepo-Coupe, N., Beringer, J., Hutley, L., Kanniah, K., Cleverly, J., Eamus, D., 2014. Parameterization of an ecosystem light-use-efficiency model for predicting savanna GPP using MODIS EVI. Remote Sens. Environ. 154, 253–271. https://doi.org/10.1016/j.rse.2014.08.025.
Major, D., Baret, F., Guyot, G., 1990. International Journal of Remote Sensing A ratio vegetation index adjusted for soil brightness. Int. J. Remote Sens. 11, 727–740.
Meyer, G.E., Neto, J.C., 2008. Verification of color vegetation indices for automated crop imaging applications. Comput. Electron. Agric. 63, 282–293.
Montero, D., Aybar, C., Mahecha, M., Martinuzzi, F., Söchting, M., Wieneke, S., 2023. A standardized catalogue of spectral indices to advance the use of remote sensing in earth system research. Sci. Data 10, 197. https://doi.org/10.1038/s41597-023-02096-0.
Mutanga, O., Skidmore, A., 2004. Narrow band vegetation indices overcome the saturation problem in biomass estimation. Int. J. Remote Sens. 25, 3999–4014. https://doi.org/10.1080/01431160310001654923.
Mutanga, O., Masenyama, A., Sibanda, M., 2023. Spectral saturation in the remote sensing of high-density vegetation traits: a systematic review of progress, challenges, and prospects. ISPRS J. Photogramm. Remote Sens. 198, 297–309. https://doi.org/10.1016/j.isprsjprs.2023.03.010.
Myneni, R.B., Hoffman, S., Knyazikhin, Y., Privette, J.L., Glassy, J.M., Tian, Y., Wang, Y., Song, X., Zhang, Y., Smith, G.R., Lotsch, A., Friedl, M., Morisette, J.T., Votava, P., Nemani, R., Running, S., 2002. Global products of vegetation leaf area and fraction absorbed PAR from year one of MODIS data. Remote Sens. Environ. 83, 214–231.
Nagy, A., Fehér, J., Tamás, J., 2018. Wheat and maize yield forecasting for the Tisza river catchment using MODIS NDVI time series and reported crop statistics. Comput. Electron. Agric. 151, 41–49.
Noda, H., Motohka, T., Murakami, K., Muraoka, H., Nasahara, K., 2014. Reflectance and transmittance spectra of leaves and shoots of 22 vascular plant species and reflectance spectra of trunks and branches of 12 tree species in Japan. Ecol. Res. 29, 111. https://doi.org/10.1007/s11284-013-1096-z.
Pinty, B., Verstraete, M.M., 1992. GEMI: a non-linear index to monitor global vegetation from satellites. Vegetatio 101, 15–20.
Potithep, S., Nagai, S., Nasahara, K.N., Muraoka, H., Suzuki, R., 2013. Two separate periods of the LAI-VIs relationships using in situ measurements in a deciduous broadleaf forest. Agric. For. Meteorol. 169, 148–155. https://doi.org/10.1016/j.agrformet.2012.09.003.
Pu, J., Yan, K., Zhou, G., Lei, Y., Zhu, Y., Guo, D., Li, H., Xu, L., Knyazikhin, Y., Myneni, R.B., 2020. Evaluation of the MODIS LAI/FPAR algorithm based on 3D-RTM simulations: a case study of grassland. Remote Sens. 12, 3391. https://doi.org/10.3390/rs12203391.
Qi, J., Xie, D., Guo, D., Yan, G., 2017. A large-scale emulation system for realistic three-dimensional (3-D) forest simulation. IEEE J. Select. Top. Appl. Earth Observ. Remote Sens. 10, 4834–4843.
Qi, J., Xie, D., Jiang, J., Huang, H., 2022. 3D radiative transfer modeling of structurally complex forest canopies through a lightweight boundary-based description of leaf clusters. Remote Sens. Environ. 283, 113301 https://doi.org/10.1016/j.rse.2022.113301.
Qi, J., Chehbouni, A., Huete, A., Kerr, Y., Sorooshian, S., 1994. A Modified Soil Adjusted Vegetation Index. Remote Sens. Environ. 48, 119–126.
Qi, J., Jiang, J., Zhou, K., Xie, D., Huang, H., 2023. Fast and accurate simulation of canopy reflectance under wavelength-dependent optical properties using a semi-empirical 3D radiative transfer model. J. Remote Sens. 3, 17. https://doi.org/10.34133/remotesensing.0017.
Qi, J., Xie, D., Yin, T., Yan, G., Gastellu-Etchegorry, J.-P., Li, L., Zhang, W., Mu, X., Norford, L.K., 2019. LESS: LargE-Scale remote sensing data and image simulation framework over heterogeneous 3D scenes. Remote Sens. of Environ. 221, 695–706. https://doi.org/10.1016/j.rse.2018.11.036.
Rautiainen, M., Hovi, A., Forsström, P., Juola, J., Kuusinen, N., Schraik, D., 2022. Open data sets on spectral properties of boreal forest components, p. 5194. https://doi.org/10.5194/egusphere-egu22-2711.
Regaieg, O., Yin, T., Malenovský, Z., Cook, B.D., Morton, D.C., Gastellu-Etchegorry, J.P., 2021. Assessing impacts of canopy 3D structure on chlorophyll fluorescence radiance and radiative budget of deciduous forest stands using DART. Remote Sens. Environ. 265 https://doi.org/10.1016/j.rse.2021.112673.
Richardson, A.J., Wiegand, C.L., 1977. Distinguishing vegetation from soil background information. Photogramm. Eng. Remote Sensing 43, 1541–1552.
Rikimaru, A., Roy, P.S., Miyatake, S., 2002. Tropical forest cover density mapping. Trop. Ecol. 43, 39–47.
Rondeaux, G., Steven, M., Baret, F., 1996. Optimization of soil-adjusted vegetation indices. Remote Sens. Environ. 55, 95–107. https://doi.org/10.1016/0034-4257(95)00186-7.
Roujean, J.L., Breon, F.M., 1995. Estimating PAR absorbed by vegetation from bidirectional reflectance measurements. Remote Sens. Environ. 51, 375–384. https://doi.org/10.1016/0034-4257(94)00114-3.
Rouse, J.W., Hass, R.H., Schell, J.A., Deering, D.W., 1974. Monitoring vegetation systems in the Great Plains with ERTS. Nasa ERTS Symp 309–313.
Sims, D.A., Gamon, J.A., 2002. Relationships between leaf pigment content and spectral reflectance across a wide range of species, leaf structures and developmental stages. Remote Sens. Environ. 81, 337–354. https://doi.org/10.1016/S0034-4257(02)00010-X.
Soh, L.K., Tsatsoulis, C., 1999. Texture analysis of Sar Sea ice imagery using gray level co-occurrence matrices. IEEE Trans. Geosci. Remote Sens. 37, 780–795. https://doi.org/10.1109/36.752194.
Tucker, C.J., 1979. Monitoring the grasslands of the sahel 1984-1985. Remote Sens. Environ. 8, 127–150.
Vaiopoulos, D., Skianis, G.A., Nikolakopoulos, K., 2004. The contribution of probability theory in assessing the efficiency of two frequently used vegetation indices. Int. J. Remote Sens. 25, 4219–4236. https://doi.org/10.1080/01431160410001680464.
Van Der Tol, C., Verhoef, W., Timmermans, J., Verhoef, A., Su, Z., 2009. An integrated model of soil-canopy spectral radiances, photosynthesis, fluorescence, temperature and energy balance. Biogeosciences 6, 3109–3129. https://doi.org/10.5194/bg-6-3109-2009.
Veraverbeke, S., Dennison, P., Gitas, I., Hulley, G., Kalashnikova, O., Katagis, T., Kuai, L., Meng, R., Roberts, D., Stavros, N., 2018. Hyperspectral remote sensing of fire: state-of-the-art and future perspectives. Remote Sens. Environ. 216, 105–121. https://doi.org/10.1016/j.rse.2018.06.020.
Verhoef, W., 1984. Light scattering by leaf layers with application to canopy reflectance modeling: the SAIL model. Remote Sens. Environ. 16, 125–141.
Wang, J., Cao, X., Chen, J., Jia, X., 2015. Assessment of multiple scattering in the reflectance of semiarid shrublands. IEEE Trans. Geosci. Remote Sens. 53, 4910–4921. https://doi.org/10.1109/TGRS.2015.2413409.
Weiss, M., Baret, F., 1999. Evaluation of canopy biophysical variable retrieval performances from the accumulation of large swath satellite data. Remote Sens. Environ. 70, 293–306. https://doi.org/10.1016/S0034-4257(99)00045-0.
Widlowski, J.-L., Lavergne, T., Pinty, B., Verstraete, M.M., Gobron, N., 2006. Rayspread: A Virtual Laboratory for Rapid BRF Simulations over 3-D Plant Canopies.

Wu, C., Niu, Z., Tang, Q., Huang, W., 2008. Estimating chlorophyll content from hyperspectral vegetation indices: Modeling and validation. Agric. For. Meteorol. 148, 1230–1241.

Xing, N., Huang, W., Xie, Q., Shi, Y., Ye, H., Dong, Y., Wu, M., Sun, G., Jiao, Q., 2020. A transformed triangular vegetation index for estimating winter wheat leaf area index. Remote Sens. 12, 1–19. https://doi.org/10.3390/RS12010016.

Yan, K., Gao, S., Chi, H., Qi, J., Song, W., Tong, Y., Mu, X., Yan, G., 2020. Evaluation of the vegetation-index-based dimidiate pixel model for fractional vegetation cover estimation. IEEE Trans. Geosci. Remote Sens. 60, 1–14. https://doi.org/10.1109/TGRS.2020.3048493.

Yan, K., Pu, J., Park, T., Xu, B., Zeng, Y., Yan, G., Weiss, M., Knyazikhin, Y., Myneni, R.B., 2021. Performance stability of the MODIS and VIIRS LAI algorithms inferred from analysis of long time series of products. Remote Sens. Environ. 260, 112438 https://doi.org/10.1016/j.rse.2021.112438.

Yao, Y., Liu, Q., Liu, Q., Li, X., 2008. LAI retrieval and uncertainty evaluations for typical row-planted crops at different growth stages. Remote Sens. Environ. 112, 94–106. https://doi.org/10.1016/j.rse.2006.09.037.

Zeng, Y., Hao, D., Huete, A., Dechant, B., Berry, J., Chen, J.M., Chen, M., 2022. Optical vegetation indices for monitoring terrestrial ecosystems globally. Nat. Rev. Earth Environ. 3, 477–493. https://doi.org/10.1038/s43017-022-00298-5.

Zhang, H., Jiao, Z., Liu, P., Dong, Y., Lian, Y., Huo, H.-Y., Cui, T., 2016. Assessment of the correlation between reflectance anisotropy and NDVI using MODIS BRDF product. In: 2016 IEEE International Geoscience and Remote Sensing Symposium (IGARSS). IEEE, pp. 1284–1287. https://doi.org/10.1109/IGARSS.2016.7729326.

Zhao, J., Li, J., Liu, Q., Yang, L., 2012. A Preliminary Study on Mechanism of Lai Inversion Saturation. The International Archives of the Photogrammetry, Remote Sensing and Spatial Information Sciences XXXIX-B1, pp. 77–81. https://doi.org/10.5194/isprsarchives-xxxix-b1-77-2012.

Zhen, Z., Chen, S., Yin, T., Chavanon, E., Lauret, N., Guilleux, J., Henke, M., Qin, W., Cao, L., Li, J., Lu, P., Gastellu-etchegorry, J.P., 2021. Using the negative soil adjustment factor of soil adjusted vegetation index (SAVI) to resist saturation effects and estimate leaf area index (LAI) in dense vegetation areas. Sensors 21, 2155. https://doi.org/10.3390/s21062115.